Ninth International Conference on Computational Fluid Dynamics (ICCFD9), Istanbul, Turkey, July 11-15, 2016

ICCFD9-2016-115

On the freestream preservation of the high order WENO scheme in general curvilinear coordinates

Yujie Zhu[1], Zhensheng Sun[1,2,*], Yuxin, Ren[2] , Yu Hu [1], Shiying Zhang[1]

1 Xi'an Research Institute of High-tech, Xi'an Shaanxi 710025, China
2 Department of Mechanics, Tsinghua University, Beijing 100084, China

*Corresponding author: szs07@mails.tsinghua.edu.cn

Abstract: The weighted essentially non-oscillatory (WENO) schemes have been extensively employed for the simulation of complex flow fields due to their high order accuracy and good shock-capturing properties. However, the standard finite difference WENO schemes cannot hold freestream in general curvilinear coordinates even by using the conservative metric method (CMM) and symmetrical conservative metric method (SCMM) developed by Deng et al[16]. The reasons are reconfirmed in the present paper: (1) the numerical derivative operators for the fluxes are nonlinear ones and (2) more importantly, the flux operators depend on the difference operators for the metrics. Errors from non-preserved freestream can hide small scales such as turbulent flow structures, aero-acoustic waves which make the results inaccuracy or even cause the simulation failure. To copy with this problem, a new numerical strategy to ensure freestream preservation properties of the WENO schemes on the stationary curvilinear grids is adopted in the present paper. This strategy includes the following procedures: (1) the metric invariants are retained in the governing equations and the full forms of the transformed equations on the general curvilinear coordinates are solved; (2) the symmetrical, conservative form of the metrics instead of the original ones are used; (3) the WENO schemes which are applied for the fluxes of the governing equations are employed to compute the outer-level partial derivatives of the metric invariants. It is verified theoretically in this paper that by using this approach, the WENO schemes hold the freestream preservation properties naturally and thus work well in the generalized coordinate systems. For some well-known WENO schemes, the derivative operators for the metric invariants are explicitly expressed and thus this approach can be straightforwardly employed. The effectiveness of this strategy is validated by several benchmark test cases. Turkey in July 11-15, 2015.

Keywords: Geometrical conservation law, WENO schemes, Nonlinear schemes, Freestream preservation.

1 Introduction

With the development of the computational fluid dynamics (CFD), high order schemes have been widely employed for the direct numerical simulation (DNS) and large eddy simulation (LES) of flow fields with a broadband of length scales such as turbulence, aero-acoustics, etc. Comparing with finite volume schemes, finite difference schemes are more computational efficiency and are easier to achieve high order accuracy. It has been reported that for a three-dimensional turbulence problem, the finite difference scheme costs one-tenth computational time comparing to the finite volume scheme with the same order of accuracy[1]. Moreover, the high order finite volume methods require multi-dimensional reconstruction procedures while the finite difference schemes can be constructed in a dimension-by-dimension manner. Thus, the finite difference schemes are much easier to be implemented on a parallel processing computer. Therefore, high order finite difference schemes retrieve the favor of scientific researchers and have been widely developed since 1990s. These includes the compact schemes[2], the weighted compact nonlinear scheme (WCNS)[3] and the weighted essentially non-oscillatory (WENO) scheme in finite difference version[4], etc.

However, finite difference schemes are usually derived on uniformly spaced grids in Castesian coordinates. When they are applied to general curvilinear coordinates, freestream preservation properties cannot be hold as the geometric conservation law (GCL) cannot be satisfied naturally. In this case, the geometrically induced errors degrade the fidelity and accuracy of the high order schemes or even cause numerical instabilities[5][6]. To eliminate or reduce such geometrically induced errors, special strategies should be adopted for the discretization of the metric terms to make the schemes fulfill the GCL. Besides, large computational time step will be allowed if a numerical algorithm satisfying GCL, which will save vast calculating resources [7].

In fact, GCL has been discussed for a long period. The concept was first proposed by Trulio and Trigger[8]. Pulliam and Steger[10] recognized that when the finite difference schemes are used to solve the three-dimensional strong conservative equations on curvilinear coordinates, errors will be introduced due to the discretization of the metrics terms. Thomas and Lombard[5] derived a conservative form of the metrics which are analytically equivalent and numerically consistent. By using the metric terms in conservative form, the geometrically induced errors are reduced in a large extent. Zhang et al. [9] pointed out that the GCL identities comprise two parts: the volume conservation law (VCL) and the surface conservation law (SCL). VCL is mainly responsible for the extra sources or sinks in the physically conservative media while the misrepresentation of the convective velocities will be caused if the SCL is not satisfied. For moving grids, many researchers have done a lot of work to satisfy the VCL. For example, Farhat et al.[11] proved that it was a necessary and sufficient condition for ALE methods to satisfy GCL in order to preserve the nonlinear stability of their fixed grid counterpart. Étienne et al.[7]and Mavriplis et al.[12] presented new approaches for ALE finite element methods to preserve freestream. Recently, Sjögreen et al.[13] proposed a systematic formulation of conservative metric discretization which satisfied GCL on moving grids. They discussed a wide class of temporal metric discretization and constructed multistage Runge-Kutta methods which satisfied the GCL identity. For the stationary curvilinear grids, the SCL identity is very important[9]. Many techniques for low-order schemes to satisfy SCL have been devised, such as a simple averaging and differencing method proposed by Pulliam and Steger[10] and a finite-volume like technique employed by Vinokur[6]. However, these methods just work well for schemes with second order accuracy. When they are employed for high order schemes, the effects are marginal. In order to make the high-order schemes satisfy GCL, Visbal and Gaitonde[14] carefully studied metrics induced errors and concluded that the errors can be largely decreased by a two-step procedures. Firstly, the conservative forms of the metric derivatives suggested by Thomas and Lambard[5] are used instead of their original forms. Secondly, the same numerical scheme is employed to calculate the metric derivatives and the flux derivatives. They successfully applied this approach to the linear central-type compact schemes. Nonomura et al.[15] extended this method to the nonlinear WCNS schemes and showed excellent freestream preservation properties of these schemes. Deng et al [16] analyzed this methodology theoretically and presented a conservative metric method (CMM) for the high order schemes to satisfy SCL. They proved that CMM is a sufficient condition for SCL and can ensure the SCL for both the interior schemes and the near boundary schemes. In their paper, the finite difference schemes are categorized as central schemes (CS) and upwind schemes (UPS) based on the difference operators which are used for the computation of the flux derivatives. They concluded that CMM can be applied to CS but cannot be applied to UPS directly. Later, Deng et al.[17] further discussed the metrics terms by following the concept of vectorized surface and cell volume in finite volume methods. They found that the discretization of metrics terms in conservative form is identical with a linear combination of the vectorized surface and cell volume around the computational nodes. Based on these discussions, they proposed the symmetrical conservative metric method (SCMM) to calculate metrics and Jacobian. Similar idea was also shown by Abe et al.[18] who proposed a new analytical forms for the metrics and Jacobian which was called asymmetric conservative metrics. The sufficient condition of a linear high order finite difference scheme was derived by Abe et al.[19], for which the conservative metrics in discrete form satisfying the GCL identity on moving and deforming grids. Under the guidelines discussed above, lots of finite difference schemes which satisfy GCL have been newly devised[20][21].

Among various high order finite difference schemes, the WENO schemes are promising due to their high order accuracy and robust shock-capturing properties. However, it has been demonstrated that the standard finite difference WENO schemes cannot satisfy the GCL when they are directly employed in a body-fitted coordinates[15][22]. Specific treatments have to be done to make the WENO schemes hold freestream. Unfortunately, the CMM cannot be applied to WENO schemes as they fall into UPS due to Deng's categories[16]. We further study the characteristic of the WENO scheme in the present paper and find that CMM cannot be used to WENO schemes owing to two reasons. Firstly, the difference operators δ_1 which are used for physical fluxes are related to the distribution of the flow field, i.e., they are nonlinear operators. Secondly, the flux operators δ_1 depend on the metric operators δ_2 which make it is impossible to design $\delta_2 = \delta_1$. Jiang et al.[23][24] proposed an alternative finite-difference form of WENO (AWENO) scheme for freestream preservation. However, Asahara et al.[25] demonstrated that the AWENO scheme is analytically equivalent to a special case of WCNS which fall into CS. Nonomura et al.[26] proposed a new technique called WENO-FP scheme to preserve freestream for the standard finite difference WENO schemes. They divided the WENO scheme into two parts: a consistent central (linear) part and a numerical dissipation (nonlinear) part. For the linear part, the CMM approach can be directly adopted. For the nonlinear part, the metric terms are frozen for constructing the upwinding fluxes.

In the present paper, a new numerical strategy is developed for the WENO scheme to satisfy the GCL. This method includes the following procedures. Firstly, the metric invariants are retained in the governing equations and the full forms of the transformed equations on the general curvilinear coordinates are solved. Secondly, the metric terms and the Jacobian are rewritten into the symmetrical conservative, analytically identical form[17][18]. Thirdly, the evaluation of any outer-level derivatives appearing in metric invariants is carried out by using an upwind-weighted averaging procedure. The characteristic-wise, fifth-order WENO scheme with Lax-Friedrich splitting is chosen as an example to shown the performance of the proposed methodology. The detailed formulations for the discretization of the metric invariants are explicit expressed. The effectiveness of this approach is validated by both theoretical analysis and benchmark test cases. The extension of this technique to other nonlinear schemes is trivial.

This thesis is organized as follows. In Section 2, the three-dimensional scalar conservation law is employed to briefly illustrate the headstream of the geometrical induced errors. Section 3.1 briefly reviews the WENO schemes on curvilinear coordinates. The reasons why standard WENO scheme cannot hold freestream are also expressed in detail in this section. A new methodology for the WENO scheme to preserve the freestream on stationary curvilinear grids is proposed in Section 3.2 and its extension to Euler and Navier-Stokes equations is given in Section 3.3. Section 4 describes some benchmark test cases to demonstrate the effectiveness of the proposed approach. The conclusions are given in Section 5.

2 General theory

2.1 Governing equations and coordinate transformations

In Cartesian coordinates (x, y, z, t), the three-dimensional scalar conservation law can be written as

$$u_t + f(u)_x + g(u)_y + h(u)_z = 0, \tag{1}$$

where u is a conservative variable while f, g and h are its fluxes. The subscripts denote the partial derivatives. For example, u_t denotes the partial derivative $\partial u/\partial t$. When the flow fields around an arbitrary body shape are simulated by finite difference schemes, Eq.(1) is usually transformed into general curvilinear coordinates (ξ, η, ζ, τ) by using the following relationships

$$\tau = t \quad \xi = \xi(x, y, z, t) \quad \eta = \eta(x, y, z, t) \quad \zeta = \zeta(x, y, z, t). \tag{2}$$

After transformation, Eq.(1) can be expressed as[27]

$$\tilde{u}_\tau + \tilde{f}_\xi + \tilde{g}_\eta + \tilde{h}_\zeta = \tilde{R}, \tag{3}$$

where

$$\begin{aligned}
\tilde{u} &= \frac{u}{J} \\
\tilde{f} &= \frac{\xi_t}{J}u + \frac{\xi_x}{J}f + \frac{\xi_y}{J}g + \frac{\xi_z}{J}h \\
\tilde{g} &= \frac{\eta_t}{J}u + \frac{\eta_x}{J}f + \frac{\eta_y}{J}g + \frac{\eta_z}{J}h \\
\tilde{h} &= \frac{\zeta_t}{J}u + \frac{\zeta_x}{J}f + \frac{\zeta_y}{J}g + \frac{\zeta_z}{J}h
\end{aligned}. \tag{4}$$

In Eq.(4), the Jacobian $1/J$ and the traditional standard metrics are defined as

$$\begin{aligned}
&1/J = \frac{\partial(x, y, z)}{\partial(\xi, \eta, \zeta)} = x_\xi y_\eta z_\zeta - x_\eta y_\xi z_\zeta + x_\zeta y_\xi z_\eta - x_\xi y_\zeta z_\eta + x_\eta y_\zeta z_\xi - x_\zeta y_\eta z_\xi \\
&\xi_x/J = y_\eta z_\zeta - y_\zeta z_\eta,\ \ \xi_y/J = x_\zeta z_\eta - x_\eta z_\zeta,\ \ \xi_z/J = x_\eta y_\zeta - x_\zeta y_\eta \\
&\eta_x/J = y_\zeta z_\xi - y_\xi z_\zeta,\ \ \eta_y/J = x_\xi z_\zeta - x_\zeta z_\xi,\ \ \eta_z/J = x_\zeta y_\xi - x_\xi y_\zeta \\
&\zeta_x/J = y_\xi z_\eta - y_\eta z_\xi,\ \ \zeta_y/J = x_\eta z_\xi - x_\xi z_\eta,\ \ \zeta_z/J = x_\xi y_\eta - x_\eta y_\xi
\end{aligned}. \tag{5}$$

$\tilde{R}$ in Eq.(3) is known as the metric invariants of the transformation. Its detailed formulation can be expressed as

$$\tilde{R} = I_t u + I_x f + I_y g + I_z h\,, \tag{6}$$

where

$$\begin{cases} I_t = (1/J)_t + (\xi_t/J)_\xi + (\eta_t/J)_\eta + (\zeta_t/J)_\zeta \\ I_x = (\xi_x/J)_\xi + (\eta_x/J)_\eta + (\zeta_x/J)_\zeta \\ I_y = (\xi_y/J)_\xi + (\eta_y/J)_\eta + (\zeta_y/J)_\zeta \\ I_z = (\xi_z/J)_\xi + (\eta_z/J)_\eta + (\zeta_z/J)_\zeta \end{cases}. \tag{7}$$

If the metrics relations in Eq.(5) are substituted into Eq.(7), each term of the metric invariants $\tilde{R}$ proves analytically to be zero. Therefore, $\tilde{R}$ is often discarded in the practical simulation. In this case, Eq.(3) results in the strong conservation form of the governing equations

$$\tilde{u}_\tau + \tilde{f}_\xi + \tilde{g}_\eta + \tilde{h}_\zeta = 0\,. \tag{8}$$

2.2 Geometrical Conservation Law

If a uniform flow is considered, Eq.(8) can be simplified as

$$\tilde{u}_\tau = -u\left[I_t - (1/J)_t\right] - \left(I_x f + I_y g + I_z h\right). \tag{9}$$

It is straightforward to see that if

$$I_t = 0 \tag{10}$$

and

$$I_x = I_y = I_z = 0 \tag{11}$$

hold, any uniform flow is the solution of Eq.(8). As previously discussed by Zhang et al.[9], $I_t = 0$ denotes VCL while $I_x = I_y = I_z = 0$ represents SCL. In the present paper, the time-constant grids are considered, thus VCL is satisfied automatically. In this case, the metric invariants $\tilde{R}$ change to be

$$\tilde{R} = I_x f + I_y g + I_z h\,. \tag{12}$$

Although SCL identity is analytically true, it may be broken numerically when improper derivative operators are employed to discrete the metric terms. The violation of the SCL identity brings extra errors which can lead to numerical inaccuracy, instabilities, or even cause the simulation failure. To settle this problem, Thomas and Lombard[5] firstly suggested the following conservative forms of the metrics S1 instead of their original form:

$$\begin{cases} (\xi_x/J)^{S1} = (y_\eta z)_\zeta - (y_\zeta z)_\eta, & (\xi_y/J)^{S1} = (xz_\eta)_\zeta - (xz_\zeta)_\eta, & (\xi_z/J)^{S1} = (x_\eta y)_\zeta - (x_\zeta y)_\eta \\ (\eta_x/J)^{S1} = (y_\zeta z)_\xi - (y_\xi z)_\zeta, & (\eta_y/J)^{S1} = (xz_\zeta)_\xi - (xz_\xi)_\zeta, & (\eta_z/J)^{S1} = (x_\zeta y)_\xi - (x_\xi y)_\zeta \\ (\zeta_x/J)^{S1} = (y_\xi z)_\eta - (y_\eta z)_\xi, & (\zeta_y/J)^{S1} = (xz_\xi)_\eta - (xz_\eta)_\xi, & (\zeta_z/J)^{S1} = (x_\xi y)_\eta - (x_\eta y)_\xi \end{cases}. \tag{13}$$

Hence, the numerical value of I_x can be written as

$$\begin{aligned} I_x^N = {} & \delta_1^\xi \delta_2^\zeta \left(z\delta_3^\eta y\right) - \delta_1^\xi \delta_2^\eta \left(z\delta_3^\zeta y\right) \\ & + \delta_1^\eta \delta_2^\xi \left(z\delta_3^\zeta y\right) - \delta_1^\eta \delta_2^\zeta \left(z\delta_3^\xi y\right), \\ & + \delta_1^\zeta \delta_2^\eta \left(z\delta_3^\xi y\right) - \delta_1^\zeta \delta_2^\xi \left(z\delta_3^\eta y\right) \end{aligned} \tag{14}$$

where the superscript "N" denotes the numerical value. δ_1, δ_2 and δ_3 are numerical derivative operators which are employed to calculate the corresponding level of the metric terms. Deng et al.[16]

verified that $I_x = 0$ can be maintained numerically when the following conditions are satisfied. That is

$$\delta_1^{\xi}\delta_2^{\zeta} = \delta_1^{\zeta}\delta_2^{\xi},\ \ \delta_1^{\xi}\delta_2^{\eta} = \delta_1^{\eta}\delta_2^{\xi},\ \ \delta_1^{\eta}\delta_2^{\zeta} = \delta_1^{\zeta}\delta_2^{\eta}. \tag{15}$$

According to these conditions, they developed CMM to make the finite difference schemes satisfy SCL. The essential idea of the CMM includes that (1) the conservative form of the metric terms, Eq.(10), are employed for the metric calculation and (2) the derivative operator δ_2 is the same with δ_1 which is used for the flux discretization in the same coordinate direction. When δ_1 is a linear operator, CMM can be implemented straightforwardly. Thus, this approach is successfully used in the linear schemes or some of the nonlinear schemes (such as WCNS) in which δ_1 is a linear operator. However, it is quite difficult or even impossible to use CMM to the WENO schemes owing to the following two reasons: (1) As noted by Deng et al., δ_1 is a nonlinear operator in WENO schemes; (2) More importantly, δ_1 depends on δ_2 which makes it is impossible to design the operator $\delta_2 = \delta_1$. Detailed discussions about this point are shown in the following section and a numerical approach to make the WENO schemes hold freestream on the stationary grids is thus devised.

3 A methodology for WENO schemes holding freestream

3.1 Analysis for the WENO schemes

The semi-discrete approximation of the governing equations in strong conservation form, Eq.(8), can be written as

$$\left(\frac{\partial \tilde{u}}{\partial \tau}\right)_{i,j,k} = -\left(\delta_1^{\xi}\tilde{f}_{i,j,k} + \delta_1^{\eta}\tilde{g}_{i,j,k} + \delta_1^{\zeta}\tilde{h}_{i,j,k}\right). \tag{16}$$

where δ_1^{ξ}, δ_1^{η} and δ_1^{ζ} are different derivative operators in $\xi-$, $\eta-$ and $\zeta-$ direction respectively. Suppose $\Delta\xi = \Delta\eta = \Delta\zeta = 1$ on the computational mesh, then $\delta_1^{\xi}\tilde{f}_{i,j,k}$ can be expressed as

$$\delta_1^{\xi}\tilde{f}_{i,j,k} = \hat{f}_{i+1/2,j,k} - \hat{f}_{i-1/2,j,k}, \tag{17}$$

where $\hat{f}_{i+1/2,j,k}$ and $\hat{f}_{i-1/2,j,k}$ are the numerical fluxes computed by the WENO schemes. Without loss of generality, the fifth order WENO scheme with Lax-Friedrichs flux splitting approach is employed in the present paper to derive the difference operator δ_1^{ξ}. Firstly, the upwinding flux $\tilde{f}_i^{+}$ (the subscript j, k are omitted for brevity where there is no ambiguity in this subsection) and the downwinding flux $\tilde{f}_i^{-}$ are split at the grid points. That is

$$\tilde{f}_i^{\pm} = \frac{1}{2}\left(\tilde{f}_i \pm \alpha\tilde{u}_i\right), \tag{18}$$

where α is taken as

$$\alpha = \max_u \left|\tilde{f}'(\tilde{u})\right| \tag{19}$$

over the relevant range of $\tilde{u}$. Then the numerical flux can be computed by

$$\hat{f}_{i+1/2}^{\pm} = \sum_{k=0}^{2}\omega_k^{\pm}q_k^{\pm}, \tag{20}$$

where $q_k^{\pm}$ is a third-order approximation of the numerical flux on the $k-th$ stencil. Their detailed formulations are

$$q_0^+ = \frac{1}{3}\tilde{f}_{i-2}^+ - \frac{7}{6}\tilde{f}_{i-1}^+ + \frac{11}{6}\tilde{f}_i^+ \quad q_1^+ = -\frac{1}{6}\tilde{f}_{i-1}^+ + \frac{5}{6}\tilde{f}_i^+ + \frac{1}{3}\tilde{f}_{i+1}^+ \quad q_2^+ = \frac{1}{3}\tilde{f}_i^+ + \frac{5}{6}\tilde{f}_{i+1}^+ - \frac{1}{6}\tilde{f}_{i+2}^+$$
$$q_0^- = -\frac{1}{6}\tilde{f}_{i-1}^- + \frac{5}{6}\tilde{f}_i^- + \frac{1}{3}\tilde{f}_{i+1}^- \quad q_1^- = \frac{1}{3}\tilde{f}_i^- + \frac{5}{6}\tilde{f}_{i+1}^- - \frac{1}{6}\tilde{f}_{i+2}^- \quad q_2^- = \frac{11}{6}\tilde{f}_{i+1}^- - \frac{7}{6}\tilde{f}_{i+2}^- + \frac{1}{3}\tilde{f}_{i+3}^- . \tag{21}$$

$\omega_k^\pm$ are the nonlinear weights corresponding to the stencil k. For $k = 0,1,2$,

$$\omega_k^\pm = \frac{C_k^\pm}{(\varepsilon + \beta_k^\pm)^2} \bigg/ \sum_{r=0}^{2} \frac{C_r^\pm}{(\varepsilon + \beta_r^\pm)^2}, \tag{22}$$

where $C_k^\pm$ are the ideal weights and their corresponding values are

$$C_0^+ = \frac{1}{10} \quad C_1^+ = \frac{3}{5} \quad C_2^+ = \frac{3}{10}$$
$$C_0^- = \frac{3}{10} \quad C_1^- = \frac{3}{5} \quad C_1^+ = \frac{1}{10} . \tag{23}$$

$\beta_k^\pm$ are the smoothness indicators of the $k-th$ stencil and ε is a small positive parameter which is usually chosen to be $\varepsilon = 10^{-6}$. By using Eq.(20) ~ Eq.(23), the numerical flux $\hat{f}_{i+1/2}$ can be obtained. That is

$$\begin{aligned}
\hat{f}_{i+1/2} = {} & \tilde{f}_{i-2}\left(\frac{1}{6}\omega_0^+\right) + \tilde{f}_{i-1}\left(-\frac{7}{12}\omega_0^+ - \frac{1}{12}\omega_1^+ - \frac{1}{12}\omega_0^-\right) + \tilde{f}_i\left(\frac{11}{12}\omega_0^+ + \frac{5}{12}\omega_1^+ + \frac{1}{6}\omega_2^+ + \frac{5}{12}\omega_0^- + \frac{1}{6}\omega_1^-\right) \\
& + \tilde{f}_{i+1}\left(\frac{1}{6}\omega_1^+ + \frac{5}{12}\omega_2^+ + \frac{1}{6}\omega_0^- + \frac{5}{12}\omega_1^- + \frac{11}{12}\omega_2^-\right) + \tilde{f}_{i+2}\left(-\frac{1}{12}\omega_2^+ - \frac{1}{12}\omega_1^- - \frac{7}{12}\omega_2^-\right) + \tilde{f}_{i+3}\left(\frac{1}{6}\omega_2^-\right) \\
& + \alpha\tilde{u}_{i-2}\left(\frac{1}{6}\omega_0^+\right) + \alpha\tilde{u}_{i-1}\left(-\frac{7}{12}\omega_0^+ - \frac{1}{12}\omega_1^+ + \frac{1}{12}\omega_0^-\right) + \alpha\tilde{u}_i\left(\frac{11}{12}\omega_0^+ + \frac{5}{12}\omega_1^+ + \frac{1}{6}\omega_2^+ - \frac{5}{12}\omega_0^- - \frac{1}{6}\omega_1^-\right) \\
& + \alpha\tilde{u}_{i+1}\left(\frac{1}{6}\omega_1^+ + \frac{5}{12}\omega_2^+ - \frac{1}{6}\omega_0^- - \frac{5}{12}\omega_1^- - \frac{11}{12}\omega_2^-\right) + \alpha\tilde{u}_{i+2}\left(-\frac{1}{12}\omega_2^+ + \frac{1}{12}\omega_1^- + \frac{7}{12}\omega_2^-\right) + \alpha\tilde{u}_{i+3}\left(-\frac{1}{6}\omega_2^-\right)
\end{aligned} . \tag{24}$$

Then the derivative operator δ_1^ξ can be explicitly expressed as

$$\begin{aligned}
\delta_1^\xi \tilde{f}_i = {} & \hat{f}_{i+1/2} - \hat{f}_{i-1/2} \\
= {} & \tilde{f}_{i-3}\left(-\frac{1}{6}\omega_0^+\right) + \tilde{f}_{i-2}\left(\frac{3}{4}\omega_0^+ + \frac{1}{12}\omega_1^+ + \frac{1}{12}\omega_0^-\right) + \tilde{f}_{i-1}\left(-\frac{3}{2}\omega_0^+ - \frac{1}{2}\omega_1^+ - \frac{1}{6}\omega_2^+ - \frac{1}{2}\omega_0^- - \frac{1}{6}\omega_1^-\right) \\
& + \tilde{f}_i\left(\frac{11}{12}\omega_0^+ + \frac{1}{4}\omega_1^+ - \frac{1}{4}\omega_2^+ + \frac{1}{4}\omega_0^- - \frac{1}{4}\omega_1^- - \frac{11}{12}\omega_2^-\right) + \tilde{f}_{i+1}\left(\frac{1}{6}\omega_1^+ + \frac{1}{2}\omega_2^+ + \frac{1}{6}\omega_0^- + \frac{1}{2}\omega_1^- + \frac{3}{2}\omega_2^-\right) \\
& + \tilde{f}_{i+2}\left(-\frac{1}{12}\omega_2^+ - \frac{1}{12}\omega_1^- - \frac{3}{4}\omega_2^-\right) + \tilde{f}_{i+3}\left(\frac{1}{6}\omega_2^-\right) \\
& + \alpha\tilde{u}_{i-3}\left(-\frac{1}{6}\omega_0^+\right) + \alpha\tilde{u}_{i-2}\left(\frac{3}{4}\omega_0^+ + \frac{1}{12}\omega_1^+ - \frac{1}{12}\omega_0^-\right) + \alpha\tilde{u}_{i-1}\left(-\frac{3}{2}\omega_0^+ - \frac{1}{2}\omega_1^+ - \frac{1}{6}\omega_2^+ + \frac{1}{2}\omega_0^- + \frac{1}{6}\omega_1^-\right) \\
& + \alpha\tilde{u}_i\left(\frac{11}{12}\omega_0^+ + \frac{1}{4}\omega_1^+ - \frac{1}{4}\omega_2^+ - \frac{1}{4}\omega_0^- + \frac{1}{4}\omega_1^- + \frac{11}{12}\omega_2^-\right) + \alpha\tilde{u}_{i+1}\left(\frac{1}{6}\omega_1^+ + \frac{1}{2}\omega_2^+ - \frac{1}{6}\omega_0^- - \frac{1}{2}\omega_1^- - \frac{3}{2}\omega_2^-\right) \\
& + \alpha\tilde{u}_{i+2}\left(-\frac{1}{12}\omega_2^+ + \frac{1}{12}\omega_1^- + \frac{3}{4}\omega_2^-\right) + \alpha\tilde{u}_{i+3}\left(-\frac{1}{6}\omega_2^-\right)
\end{aligned} . \tag{25}$$

If we introduce the translation operator in $\xi-$direction

$$E_\beta^\xi\left(\phi_{i,j,k}\right) = \phi_{i+\beta,j,k} \tag{26}$$

and define

$$
\begin{aligned}
&w_{-3}^{\xi,+}\left(\phi_{i,j,k}\right)=-\frac{1}{6}\omega_0^{+}E_{-3}^{\xi}\left(\phi_{i,j,k}\right) \quad w_{-3}^{\xi,-}\left(\phi_{i,j,k}\right)=0\\
&w_{-2}^{\xi,+}\left(\phi_{i,j,k}\right)=\left(\frac{3}{4}\omega_0^{+}+\frac{1}{12}\omega_1^{+}\right)E_{-2}^{\xi}\left(\phi_{i,j,k}\right) \quad w_{-2}^{\xi,-}\left(\phi_{i,j,k}\right)=\left(\frac{1}{12}\omega_0^{-}\right)E_{-2}^{\xi}\left(\phi_{i,j,k}\right)\\
&w_{-1}^{\xi,+}\left(\phi_{i,j,k}\right)=\left(-\frac{3}{2}\omega_0^{+}-\frac{1}{2}\omega_1^{+}-\frac{1}{6}\omega_2^{+}\right)E_{-1}^{\xi}\left(\phi_{i,j,k}\right) \quad w_{-1}^{\xi,-}\left(\phi_{i,j,k}\right)=\left(-\frac{1}{2}\omega_0^{-}-\frac{1}{6}\omega_1^{-}\right)E_{-1}^{\xi}\left(\phi_{i,j,k}\right)\\
&w_{0}^{\xi,+}\left(\phi_{i,j,k}\right)=\left(\frac{11}{12}\omega_0^{+}+\frac{1}{4}\omega_1^{+}-\frac{1}{4}\omega_2^{+}\right)E_{0}^{\xi}\left(\phi_{i,j,k}\right) \quad w_{0}^{\xi,-}\left(\phi_{i,j,k}\right)=\left(\frac{1}{4}\omega_0^{-}-\frac{1}{4}\omega_1^{-}-\frac{11}{12}\omega_2^{-}\right)E_{0}^{\xi}\left(\phi_{i,j,k}\right)\\
&w_{1}^{\xi,+}\left(\phi_{i,j,k}\right)=\left(\frac{1}{6}\omega_1^{+}+\frac{1}{2}\omega_2^{+}\right)E_{1}^{\xi}\left(\phi_{i,j,k}\right) \quad w_{1}^{\xi,-}\left(\phi_{i,j,k}\right)=\left(\frac{1}{6}\omega_0^{-}+\frac{1}{2}\omega_1^{-}+\frac{3}{2}\omega_2^{-}\right)E_{1}^{\xi}\left(\phi_{i,j,k}\right)\\
&w_{2}^{\xi,+}\left(\phi_{i,j,k}\right)=\left(-\frac{1}{12}\omega_2^{+}\right)E_{2}^{\xi}\left(\phi_{i,j,k}\right) \quad w_{2}^{\xi,-}\left(\phi_{i,j,k}\right)=\left(-\frac{1}{12}\omega_1^{-}-\frac{3}{4}\omega_2^{-}\right)E_{2}^{\xi}\left(\phi_{i,j,k}\right)\\
&w_{3}^{\xi,+}\left(\phi_{i,j,k}\right)=0 \quad w_{3}^{\xi,-}\left(\phi_{i,j,k}\right)=\left(\frac{1}{6}\omega_2^{-}\right)E_{3}^{\xi}\left(\phi_{i,j,k}\right)
\end{aligned}
\quad ,(27)
$$

the derivative operator δ_1^{ξ} can be rewritten as

$$
\delta_1^{\xi}\tilde{f}_{i,j,k}=\sum_{r=-3}^{3}\left[w_r^{\xi,+}\left(\tilde{f}_{i,j,k}+\alpha\tilde{u}_{i,j,k}\right)+w_r^{\xi,-}\left(\tilde{f}_{i,j,k}-\alpha\tilde{u}_{i,j,k}\right)\right]. \tag{28}
$$

From above discussions, it can be clearly observed that δ_1 is a nonlinear operator as the nonlinear weights $\omega_k^{\pm}$ depend on the flow variables. Moreover, if we want to obtain δ_1, the difference operator for the metric terms, i.e., δ_2 in Eq.(14) should be known first. In other words, we should calculate δ_2 before we compute δ_1. However, when we choose a different δ_2 in the practical implementation, we obtain a different δ_1 because the nonlinear weights $\omega_k^{\pm}$ are function of the numerical values of the metric terms, which indicates the flux operator δ_1 depends on the metric operator δ_2 for the WENO schemes. Therefore, it is impossible to design $\delta_2=\delta_1$ and thus the CMM approach cannot be applied to the WENO schemes directly. However, if Eq.(3) instead of its strong conservative form Eq.(8) is solved by using WENO schemes, freestream preservation properties can be hold by proper discretization of the metrics invariants $\tilde{R}$. The detailed illustrations are given in the following subsection.

3.2 An approach on WENO schemes for freestream preservation

If a uniform flow is taken into consideration, i.e., u,f,g,h are constants over the flow fields. (It should be noted that $\tilde{u},\tilde{f},\tilde{g},\tilde{h}$ may be not constants due to the discretization errors of the metric terms.) By substituting Eq.(4) into Eq.(28), we obtain

$$
\begin{aligned}
\delta_1^{\xi}\tilde{f}_{i,j,k}=f&\sum_{r=-3}^{3}\left[w_r^{\xi,+}\left(\frac{\xi_x}{J}\right)_{i,j,k}+w_r^{\xi,-}\left(\frac{\xi_x}{J}\right)_{i,j,k}\right]\\
+g&\sum_{r=-3}^{3}\left[w_r^{\xi,+}\left(\frac{\xi_y}{J}\right)_{i,j,k}+w_r^{\xi,-}\left(\frac{\xi_y}{J}\right)_{i,j,k}\right]\\
+h&\sum_{r=-3}^{3}\left[w_r^{\xi,+}\left(\frac{\xi_z}{J}\right)_{i,j,k}+w_r^{\xi,-}\left(\frac{\xi_z}{J}\right)_{i,j,k}\right]\\
+\alpha u&\sum_{r=-3}^{3}\left[w_r^{\xi,+}\left(\frac{1}{J}\right)_{i,j,k}-w_r^{\xi,-}\left(\frac{1}{J}\right)_{i,j,k}\right]
\end{aligned}. \tag{29}
$$

In this case, Eq. (16) can be explicitly expressed as

$$
\begin{aligned}
\left(\frac{\partial \tilde{u}}{\partial \tau}\right)_{i,j,k} = & -f\left\{\sum_{r=-3}^{3}\left[w_r^{\xi,+}\left(\frac{\xi_x}{J}\right)_{i,j,k}+w_r^{\xi,-}\left(\frac{\xi_x}{J}\right)_{i,j,k}\right]+\sum_{r=-3}^{3}\left[w_r^{\eta,+}\left(\frac{\eta_x}{J}\right)_{i,j,k}+w_r^{\eta,-}\left(\frac{\eta_x}{J}\right)_{i,j,k}\right]+\sum_{r=-3}^{3}\left[w_r^{\zeta,+}\left(\frac{\zeta_x}{J}\right)_{i,j,k}+w_r^{\zeta,-}\left(\frac{\zeta_x}{J}\right)_{i,j,k}\right]\right\}. \\
& -g\left\{\sum_{r=-3}^{3}\left[w_r^{\xi,+}\left(\frac{\xi_y}{J}\right)_{i,j,k}+w_r^{\xi,-}\left(\frac{\xi_y}{J}\right)_{i,j,k}\right]+\sum_{r=-3}^{3}\left[w_r^{\eta,+}\left(\frac{\eta_y}{J}\right)_{i,j,k}+w_r^{\eta,-}\left(\frac{\eta_y}{J}\right)_{i,j,k}\right]+\sum_{r=-3}^{3}\left[w_r^{\zeta,+}\left(\frac{\zeta_y}{J}\right)_{i,j,k}+w_r^{\zeta,-}\left(\frac{\zeta_y}{J}\right)_{i,j,k}\right]\right\} \\
& -h\left\{\sum_{r=-3}^{3}\left[w_r^{\xi,+}\left(\frac{\xi_z}{J}\right)_{i,j,k}+w_r^{\xi,-}\left(\frac{\xi_z}{J}\right)_{i,j,k}\right]+\sum_{r=-3}^{3}\left[w_r^{\eta,+}\left(\frac{\eta_z}{J}\right)_{i,j,k}+w_r^{\eta,-}\left(\frac{\eta_z}{J}\right)_{i,j,k}\right]+\sum_{r=-3}^{3}\left[w_r^{\zeta,+}\left(\frac{\zeta_z}{J}\right)_{i,j,k}+w_r^{\zeta,-}\left(\frac{\zeta_z}{J}\right)_{i,j,k}\right]\right\} \\
& -\alpha u\left\{\sum_{r=-3}^{3}\left[w_r^{\xi,+}\left(\frac{1}{J}\right)_{i,j,k}-w_r^{\xi,-}\left(\frac{1}{J}\right)_{i,j,k}\right]+\sum_{r=-3}^{3}\left[w_r^{\eta,+}\left(\frac{1}{J}\right)_{i,j,k}-w_r^{\eta,-}\left(\frac{1}{J}\right)_{i,j,k}\right]+\sum_{r=-3}^{3}\left[w_r^{\zeta,+}\left(\frac{1}{J}\right)_{i,j,k}-w_r^{\zeta,-}\left(\frac{1}{J}\right)_{i,j,k}\right]\right\}
\end{aligned}
\tag{30}
$$

where $w_r^{\eta,\pm}$ and $w_r^{\zeta,\pm}$ are the operators in $\eta-$ and $\zeta-$ direction respectively. For example, when $r=-3$, $w_r^{\eta,\pm}$ can be expressed as

$$
w_{-3}^{\eta,+}\left(\phi_{i,j,k}\right)=-\frac{1}{6}\omega_0^{+}E_{-3}^{\eta}\left(\phi_{i,j,k}\right) \quad w_{-3}^{\eta,-}\left(\phi_{i,j,k}\right)=0 \tag{31}
$$

where E_{-3}^{η} is the translation operator in $\eta-$ direction

$$
E_{\beta}^{\eta}\left(\phi_{i,j,k}\right)=\phi_{i,j+\beta,k}\,. \tag{32}
$$

It is obvious that Eq.(30) cannot ensure $\partial\tilde{u}/\partial\tau=0$ for an arbitrary uniform flow owing to the discretization errors of the metric terms. However, if Eq.(3) instead of Eq.(8) is solved and the metric terms I_x , I_y and I_z in $\tilde{R}$ are discretized by

$$
\begin{aligned}
\left(I_x\right)_{i,j,k}^{N} = & \left\{\sum_{r=-3}^{3}\left[w_r^{\xi,+}\left(\frac{\xi_x}{J}\right)_{i,j,k}+w_r^{\xi,-}\left(\frac{\xi_x}{J}\right)_{i,j,k}\right]+\sum_{r=-3}^{3}\left[w_r^{\eta,+}\left(\frac{\eta_x}{J}\right)_{i,j,k}+w_r^{\eta,-}\left(\frac{\eta_x}{J}\right)_{i,j,k}\right]+\sum_{r=-3}^{3}\left[w_r^{\zeta,+}\left(\frac{\zeta_x}{J}\right)_{i,j,k}+w_r^{\zeta,-}\left(\frac{\zeta_x}{J}\right)_{i,j,k}\right]\right\} \\
& +\alpha\left(\frac{u}{f}\right)_{i,j,k}\left\{\sum_{r=-3}^{3}\left[w_r^{\xi,+}\left(\frac{1}{J}\right)_{i,j,k}-w_r^{\xi,-}\left(\frac{1}{J}\right)_{i,j,k}\right]\right\} \\
\left(I_y\right)_{i,j,k}^{N} = & \left\{\sum_{r=-3}^{3}\left[w_r^{\xi,+}\left(\frac{\xi_y}{J}\right)_{i,j,k}+w_r^{\xi,-}\left(\frac{\xi_y}{J}\right)_{i,j,k}\right]+\sum_{r=-3}^{3}\left[w_r^{\eta,+}\left(\frac{\eta_y}{J}\right)_{i,j,k}+w_r^{\eta,-}\left(\frac{\eta_y}{J}\right)_{i,j,k}\right]+\sum_{r=-3}^{3}\left[w_r^{\zeta,+}\left(\frac{\zeta_y}{J}\right)_{i,j,k}+w_r^{\zeta,-}\left(\frac{\zeta_y}{J}\right)_{i,j,k}\right]\right\} \\
& +\alpha\left(\frac{u}{g}\right)_{i,j,k}\left\{\sum_{r=-3}^{3}\left[w_r^{\eta,+}\left(\frac{1}{J}\right)_{i,j,k}+w_r^{\eta,-}\left(\frac{1}{J}\right)_{i,j,k}\right]\right\} \\
\left(I_z\right)_{i,j,k}^{N} = & \left\{\sum_{r=-3}^{3}\left[w_r^{\xi,+}\left(\frac{\xi_z}{J}\right)_{i,j,k}+w_r^{\xi,-}\left(\frac{\xi_z}{J}\right)_{i,j,k}\right]+\sum_{r=-3}^{3}\left[w_r^{\eta,+}\left(\frac{\eta_z}{J}\right)_{i,j,k}+w_r^{\eta,-}\left(\frac{\eta_z}{J}\right)_{i,j,k}\right]+\sum_{r=-3}^{3}\left[w_r^{\zeta,+}\left(\frac{\zeta_z}{J}\right)_{i,j,k}+w_r^{\zeta,-}\left(\frac{\zeta_z}{J}\right)_{i,j,k}\right]\right\} \\
& +\alpha\left(\frac{u}{h}\right)_{i,j,k}\left\{\sum_{r=-3}^{3}\left[w_r^{\zeta,+}\left(\frac{1}{J}\right)_{i,j,k}+w_r^{\zeta,-}\left(\frac{1}{J}\right)_{i,j,k}\right]\right\}
\end{aligned}
\quad , \tag{33}
$$

the discretization error of the fluxes can be exactly offset by the discretization error of $\tilde{R}$. Therefore, $\partial\tilde{u}/\partial\tau=0$ is true for any uniform flow and the WENO schemes preserve the freestream.

Remark 1: It should be noted that for this technique, the numerical values of I_x , I_y and I_z cannot be guaranteed to be zero. However, when the freestream is imposed, the numerical errors induced in the discretization of the fluxes are exactly equal to the numerical value of the metric invariants. Thus, the geometrically induced errors are offset by the disctetization of the metric invariants and $\partial\tilde{u}/\partial\tau=0$ holds for any uniform flow.

Remark 2: Theoretically, when the same numerical value of the metric terms such as ξ_x/J , ξ_y/J and ξ_z/J are employed for the discretization of the physical fluxes and the metric invariants, $\partial\tilde{u}/\partial\tau=0$ is achieved. In other words, whether the conservative forms of the metric terms are chosen or not have no effects on the freestream preservation properties of the WENO schemes for this technique. However, our experiences show that it is a smart choice to choose the metric terms in conservative forms.

Remark 3: After the conservative forms of the metric terms are chosen, the numerical values of the metric terms should be computed before Eq.(33) is employed. In other words, δ_2 and δ_3 in Eq.

(14) should be computed numerically before Eq.(33) is carried out. Although there is no restriction on the chosen of δ_2 and δ_3, the same high order schemes are chosen for δ_2 and δ_3 in the present paper.

According to above discussions, the proposed approach of the present paper can be summarized as follows:

(1) The metric invariants $\tilde{R}$ are retained in the governing equations, i.e., Eq.(3) is solved instead of the strong conservation form of the governing equations;

(2) The symmetrical conservative form of the metrics are employed[16][18]. That is

$$\begin{aligned}
&\frac{\xi_x}{J}=\frac{1}{2}\left[\left(\frac{\xi_x}{J}\right)^{S1}+\left(\frac{\xi_x}{J}\right)^{S2}\right] \quad \frac{\xi_y}{J}=\frac{1}{2}\left[\left(\frac{\xi_y}{J}\right)^{S1}+\left(\frac{\xi_y}{J}\right)^{S2}\right] \quad \frac{\xi_z}{J}=\frac{1}{2}\left[\left(\frac{\xi_z}{J}\right)^{S1}+\left(\frac{\xi_z}{J}\right)^{S2}\right]\\
&\frac{\eta_x}{J}=\frac{1}{2}\left[\left(\frac{\eta_x}{J}\right)^{S1}+\left(\frac{\eta_x}{J}\right)^{S2}\right] \quad \frac{\eta_y}{J}=\frac{1}{2}\left[\left(\frac{\eta_y}{J}\right)^{S1}+\left(\frac{\eta_y}{J}\right)^{S2}\right] \quad \frac{\eta_z}{J}=\frac{1}{2}\left[\left(\frac{\eta_z}{J}\right)^{S1}+\left(\frac{\eta_z}{J}\right)^{S2}\right],\\
&\frac{\zeta_x}{J}=\frac{1}{2}\left[\left(\frac{\zeta_x}{J}\right)^{S1}+\left(\frac{\zeta_x}{J}\right)^{S2}\right] \quad \frac{\zeta_y}{J}=\frac{1}{2}\left[\left(\frac{\zeta_y}{J}\right)^{S1}+\left(\frac{\zeta_y}{J}\right)^{S2}\right] \quad \frac{\zeta_z}{J}=\frac{1}{2}\left[\left(\frac{\zeta_z}{J}\right)^{S1}+\left(\frac{\zeta_z}{J}\right)^{S2}\right]
\end{aligned} \tag{34}$$

where the superscript "S1" denotes Eq.(13) while the superscript "S2" represents its symmetrical form:

$$\begin{cases}
(\xi_x/J)^{S2}=(yz_\zeta)_\eta-(yz_\eta)_\zeta, & (\xi_y/J)^{S2}=(x_\zeta z)_\eta-(x_\eta z)_\zeta, \quad (\xi_z/J)^{S2}=(x_\eta y)_\zeta-(x_\zeta y)_\eta\\
(\eta_x/J)^{S2}=(yz_\xi)_\zeta-(yz_\zeta)_\xi, & (\eta_y/J)^{S2}=(x_\xi z)_\zeta-(x_\zeta z)_\xi, \quad (\eta_z/J)^{S2}=(xy_\xi)_\zeta-(xy_\zeta)_\xi\\
(\zeta_x/J)^{S2}=(yz_\eta)_\xi-(yz_\xi)_\eta, & (\zeta_y/J)^{S2}=(x_\eta z)_\xi-(x_\xi z)_\eta, \quad (\zeta_z/J)^{S2}=(xy_\eta)_\xi-(xy_\xi)_\eta
\end{cases}. \tag{35}$$

The symmetrical conservative form of the Jacobian $1/J$ can be written as

$$1/J=\frac{1}{3}\left\{\begin{aligned}&\left[x(\xi_x/J)+y(\xi_y/J)+z(\xi_z/J)\right]_\xi\\ &+\left[x(\eta_x/J)+y(\eta_y/J)+z(\eta_z/J)\right]_\eta\\ &+\left[x(\zeta_x/J)+y(\zeta_y/J)+z(\zeta_z/J)\right]_\zeta\end{aligned}\right\}. \tag{36}$$

(3) Eq.(33) is employed to compute the outer-level partial derivatives in $\tilde{R}$. In other words, $\tilde{R}$ is discretized by

$$\begin{aligned}
\tilde{R}=f&\left\{\sum_{r=-3}^{3}\left[w_r^{\xi,+}\left(\frac{\xi_x}{J}\right)_{i,j,k}+w_r^{\xi,-}\left(\frac{\xi_x}{J}\right)_{i,j,k}\right]+\sum_{r=-3}^{3}\left[w_r^{\eta,+}\left(\frac{\eta_x}{J}\right)_{i,j,k}+w_r^{\eta,-}\left(\frac{\eta_x}{J}\right)_{i,j,k}\right]+\sum_{r=-3}^{3}\left[w_r^{\zeta,+}\left(\frac{\zeta_x}{J}\right)_{i,j,k}+w_r^{\zeta,-}\left(\frac{\zeta_x}{J}\right)_{i,j,k}\right]\right\}\\
+g&\left\{\sum_{r=-3}^{3}\left[w_r^{\xi,+}\left(\frac{\xi_y}{J}\right)_{i,j,k}+w_r^{\xi,-}\left(\frac{\xi_y}{J}\right)_{i,j,k}\right]+\sum_{r=-3}^{3}\left[w_r^{\eta,+}\left(\frac{\eta_y}{J}\right)_{i,j,k}+w_r^{\eta,-}\left(\frac{\eta_y}{J}\right)_{i,j,k}\right]+\sum_{r=-3}^{3}\left[w_r^{\zeta,+}\left(\frac{\zeta_y}{J}\right)_{i,j,k}+w_r^{\zeta,-}\left(\frac{\zeta_y}{J}\right)_{i,j,k}\right]\right\}\\
+h&\left\{\sum_{r=-3}^{3}\left[w_r^{\xi,+}\left(\frac{\xi_z}{J}\right)_{i,j,k}+w_r^{\xi,-}\left(\frac{\xi_z}{J}\right)_{i,j,k}\right]+\sum_{r=-3}^{3}\left[w_r^{\eta,+}\left(\frac{\eta_z}{J}\right)_{i,j,k}+w_r^{\eta,-}\left(\frac{\eta_z}{J}\right)_{i,j,k}\right]+\sum_{r=-3}^{3}\left[w_r^{\zeta,+}\left(\frac{\zeta_z}{J}\right)_{i,j,k}+w_r^{\zeta,-}\left(\frac{\zeta_z}{J}\right)_{i,j,k}\right]\right\}\\
+\alpha u&\left\{\sum_{r=-3}^{3}\left[w_r^{\xi,+}\left(\frac{1}{J}\right)_{i,j,k}-w_r^{\xi,-}\left(\frac{1}{J}\right)_{i,j,k}\right]+\sum_{r=-3}^{3}\left[w_r^{\eta,+}\left(\frac{1}{J}\right)_{i,j,k}-w_r^{\eta,-}\left(\frac{1}{J}\right)_{i,j,k}\right]+\sum_{r=-3}^{3}\left[w_r^{\zeta,+}\left(\frac{1}{J}\right)_{i,j,k}-w_r^{\zeta,-}\left(\frac{1}{J}\right)_{i,j,k}\right]\right\}
\end{aligned}. \tag{37}$$

By using this approach, it is clear that when the uniform flow is imposed, the discretization errors of the fluxes can be exactly offset by the discretization of the metric invariants and the freestream is thus preserved.

This approach can be easily extended to other WENO schemes. For the WENO schemes with Roe-type splitting, the upwinding and the downwinding fluxes at the grid points can be written as

$$\tilde{f}_i^{\pm}=\frac{1}{2}\left[\tilde{f}_i\pm\operatorname{sgn}(\alpha)\tilde{f}_i\right], \tag{38}$$

where $\alpha=\partial\tilde{f}/\partial\tilde{u}$ and $\operatorname{sgn}(\alpha)$ is the signal function with

$$\operatorname{sgn}(\alpha)=\begin{cases}1 & \alpha>0\\ 0 & \alpha=0\\ -1 & \alpha<0\end{cases}. \tag{39}$$

In this case, I_x can be computed by

$$\begin{aligned}(I_x)_{i,j,k}^N &= \left[1+\operatorname{sgn}(\alpha_{i,j,k})\right]\sum_{r=-3}^{3}\left[w_r^{\xi,+}\left(\frac{\xi_x}{J}\right)_{i,j,k}+w_r^{\eta,+}\left(\frac{\eta_x}{J}\right)_{i,j,k}+w_r^{\zeta,+}\left(\frac{\zeta_x}{J}\right)_{i,j,k}\right]\\ &+\left[1-\operatorname{sgn}(\alpha_{i,j,k})\right]\sum_{r=-3}^{3}\left[w_r^{\xi,-}\left(\frac{\xi_x}{J}\right)_{i,j,k}+w_r^{\eta,-}\left(\frac{\eta_x}{J}\right)_{i,j,k}+w_r^{\zeta,-}\left(\frac{\zeta_x}{J}\right)_{i,j,k}\right]\end{aligned}. \tag{40}$$

for the WENO schemes with Roe-type splitting holding freestream. I_y and I_z can be obtained in a similar way.

3.3 Extension to the Euler and N-S equations

In this subsection, this approach is extended to solve the Euler and Navier-Stokes equation. The three-dimensional, unsteady, compressible Euler equations are employed for the illustrations. In general curvilinear coordinate systems, they can be expressed as

$$\tilde{\mathbf{U}}_{\boldsymbol{\tau}}+\tilde{\mathbf{F}}_{\boldsymbol{\xi}}+\tilde{\mathbf{G}}_{\boldsymbol{\eta}}+\tilde{\mathbf{H}}_{\boldsymbol{\zeta}}=\tilde{\mathbf{R}}, \tag{41}$$

where $\tilde{\mathbf{U}}$ are the conservative variables, $\tilde{\mathbf{F}}$, $\tilde{\mathbf{G}}$ and $\tilde{\mathbf{H}}$ are the inviscid fluxes. Their detailed formulations can be founded, for example, in [14]. The metric invariants $\tilde{\mathbf{R}}$ on the stationary grids can be written as

$$\tilde{\mathbf{R}}=I_x\mathbf{F}+I_y\mathbf{G}+I_z\mathbf{H}, \tag{42}$$

where $\mathbf{F}$, $\mathbf{G}$ and $\mathbf{H}$ are the inviscid fluxes in the Cartesian coordinates. When the scalar WENO schemes are extended to solve Euler equations, there are in general two ways: The component-wise WENO schemes and the characteristic-wise WENO schemes. We take I_x as an example to illustrate the discretization process of $\tilde{\mathbf{R}}$ in the following section for these two types WENO schemes respectively.

(1) The component-wise WENO schemes. For the component-wise WENO schemes, we compute the numerical fluxes using the scalar WENO schemes for each component of $\tilde{\mathbf{U}}$ separately. The Lax-Friedrichs approach is also employed for the flux splitting

$$\tilde{\mathbf{F}}_{i,j,k}^{\pm}=\frac{1}{2}\left(\tilde{\mathbf{F}}_{i,j,k}\pm\alpha\tilde{\mathbf{U}}_{i,j,k}\right), \tag{43}$$

where the constant α is taken as

$$\alpha=\max_{\tilde{\mathbf{u}}}\left(\max_{1\le p\le 5}\left|\lambda_p(\tilde{\mathbf{u}})\right|\right). \tag{44}$$

In Eq.(44), $\lambda_p(\tilde{\mathbf{u}})$ are the eigenvalues of the Jacobian $\mathbf{A}=\partial\tilde{\mathbf{F}}/\partial\tilde{\mathbf{U}}$. The maximum is taken over the relevant range of $\tilde{\mathbf{U}}$. Then the difference operator δ_1^{ξ} for any component of the inviscid flux $\tilde{\mathbf{F}}$ can be written as

$$\delta_1^{\xi}\tilde{F}_{i,j,k}^{p}=\sum_{r=-3}^{3}\left[w_r^{\xi,+}\left(\tilde{F}_{i,j,k}^{p}+\alpha\tilde{U}_{i,j,k}^{p}\right)+w_r^{\xi,-}\left(\tilde{F}_{i,j,k}^{p}-\alpha\tilde{U}_{i,j,k}^{p}\right)\right], \tag{45}$$

where $\tilde{F}_{i,j,k}^{p}$ and $\tilde{U}_{i,j,k}^{p}$ is the $p-th$ component of $\tilde{\mathbf{F}}_{i,j,k}$ and $\tilde{\mathbf{U}}_{i,j,k}$ respectively.

From above discussions, it can be observed that the metric invariants should be computed in a component-by-component fashion. For example, the numerical value of I_x for the $p-th$ component of the conservative variables can be expressed as

$$\left(I_x^p\right)^N = \left\{\sum_{r=-3}^{3}\left[w_r^{\xi,+}\left(\frac{\xi_x}{J}\right)_{i,j,k} + w_r^{\xi,-}\left(\frac{\xi_x}{J}\right)_{i,j,k}\right] + \sum_{r=-3}^{3}\left[w_r^{\eta,+}\left(\frac{\eta_x}{J}\right)_{i,j,k} + w_r^{\eta,-}\left(\frac{\eta_x}{J}\right)_{i,j,k}\right] + \sum_{r=-3}^{3}\left[w_r^{\zeta,+}\left(\frac{\zeta_x}{J}\right)_{i,j,k} + w_r^{\zeta,-}\left(\frac{\zeta_x}{J}\right)_{i,j,k}\right]\right\}. \\ +\alpha\left(\frac{U^p}{F^p}\right)\left\{\sum_{r=-3}^{3}\left[w_r^{\xi,+}\left(\frac{1}{J}\right)_{i,j,k} - w_r^{\xi,-}\left(\frac{1}{J}\right)_{i,j,k}\right]\right\} \tag{46}$$

(2) The characteristic-wise WENO schemes. Taking the computation of the difference operator δ_1^ξ for the $p-th$ component of the inviscid flux $\tilde{\mathbf{F}}_{i,j,k}$ as an example, the detailed procedure involves the following steps. (Note the subscript j and k are omitted for brevity where there is no ambiguity.)

a) At each fixed $\xi_{i+1/2}$, the average state of the conservative variables $\tilde{\mathbf{U}}$ and the inviscid fluxes $\tilde{\mathbf{F}}$ are determined by the simple arithmetic mean

$$\begin{aligned} \tilde{\mathbf{U}}_{i+1/2} &= \frac{1}{2}\left(\tilde{\mathbf{U}}_i + \tilde{\mathbf{U}}_{i+1}\right) \\ \tilde{\mathbf{F}}_{i+1/2} &= \frac{1}{2}\left(\tilde{\mathbf{F}}_i + \tilde{\mathbf{F}}_{i+1}\right) \end{aligned} \tag{47}$$

or the Roe average.

b) The left eigenvectors $\tilde{\mathbf{L}}_{i+1/2}^p\left(p=1\sim 5\right)$ and the right eigenvectors $\tilde{\mathbf{R}}_{i+1/2}^p\left(p=1\sim 5\right)$ of the matrix $\tilde{\mathbf{A}} = \partial\tilde{\mathbf{F}}/\partial\tilde{\mathbf{U}}$ are computed at the average state.

c) The left eigenvectors $\tilde{\mathbf{L}}_{i+1/2}^p\left(p=1\sim 5\right)$ are employed to project the conservative variables and the inviscid fluxes into the characteristic space on the corresponding stencil of the WENO schemes. The resulting characteristic variables are

$$\begin{aligned} w_m^p &= \tilde{\mathbf{L}}_{i+1/2}^p\tilde{\mathbf{F}}_m \quad m = i-3,\cdots,i+2 \\ \varphi_m^p &= \tilde{\mathbf{L}}_{i+1/2}^p\tilde{\mathbf{U}}_m \quad m = i-3,\cdots,i+2 \end{aligned}, \tag{48}$$

where the superscript “ p ”denotes the $p-th$ component of the characteristic variables.

d) The flux splitting is carried out in the characteristic space. When the Lax-Friedrichs flux splitting approach is used, we obtain

$$w_m^{p,\pm} = \frac{1}{2}\left(w_m^p \pm \alpha\varphi_m^p\right), \tag{49}$$

where α is given by Eq.(44).

e) Perform the scalar WENO schemes for each component of the characteristic variables to obtain the corresponding numerical flux $\hat{w}_{i+1/2}^p$. That is

$$\hat{w}_{i+1/2}^p = \sum_{r=-2}^{3} w_r^+ E_r^\xi\left(w_i^p + \alpha\varphi_i^p\right) + w_r^- E_r^\xi\left(w_i^p - \alpha\varphi_i^p\right). \tag{50}$$

where

$$
\begin{array}{ll}
w_{-2}^{+}=\frac{1}{6}\omega_0^{+} & w_{-2}^{-}=0 \\
w_{-1}^{+}=\left(-\frac{7}{12}\omega_0^{+}-\frac{1}{12}\omega_1^{+}\right) & w_{-1}^{-}=\left(-\frac{1}{12}\omega_0^{-}\right) \\
w_{0}^{+}=\left(\frac{11}{12}\omega_0^{+}+\frac{5}{12}\omega_1^{+}+\frac{1}{6}\omega_2^{+}\right) & w_{0}^{-}=\left(\frac{5}{12}\omega_0^{-}+\frac{1}{6}\omega_1^{-}\right) \\
w_{1}^{+}=\left(\frac{1}{6}\omega_1^{+}+\frac{5}{12}\omega_2^{+}\right) & w_{1}^{-}=\left(\frac{1}{6}\omega_0^{-}+\frac{5}{12}\omega_1^{-}+\frac{11}{12}\omega_2^{-}\right) \\
w_{2}^{+}=\left(-\frac{1}{12}\omega_2^{+}\right) & w_{2}^{-}=\left(-\frac{1}{12}\omega_1^{-}-\frac{7}{12}\omega_2^{-}\right) \\
w_{3}^{+}=0 & w_{3}^{-}=\frac{1}{6}\omega_0^{-}
\end{array}, \tag{51}
$$

and E_r^{ξ} is the translation operator in $\xi-$direction defined by Eq.(26).

f) At last, we transform the flux $\hat{w}_{i+1/2}^{p}$ back into physical space by

$$
\hat{F}_{i+1/2}^{p}=\sum_{q=1}^{5}\tilde{R}_{i+1/2}^{p,q}\hat{w}_{i+1/2}^{q}, \tag{52}
$$

where $\hat{F}_{i+1/2}^{p}$ is the $p-th$ component of the numerical fluxes.

Substituting Eq.(48)~Eq.(50) into Eq.(52), $\hat{F}_{i+1/2}^{p}$ can be finally expressed as

$$
\hat{F}_{i+1/2}^{p}=\sum_{q=1}^{5}\tilde{R}_{i+1/2}^{p,q}\left\{\sum_{s=1}^{5}\tilde{L}_{i+1/2}^{q,s}\left[\sum_{r=-2}^{3}w_r^{+}E_r^{\xi}\left(\tilde{F}_i^{s}+\alpha\tilde{U}_i^{s}\right)+w_r^{-}E_r^{\xi}\left(\tilde{F}_i^{s}-\alpha\tilde{U}_i^{s}\right)\right]\right\}, \tag{53}
$$

where $\tilde{U}^{s}$ and $\tilde{F}^{s}$ are the $s-th$ component of $\tilde{\mathbf{U}}$ and $\tilde{\mathbf{F}}$ respectively. If uniform flow is considered, the numerical flux can be simplified to be

$$
\hat{F}_{i+1/2}^{p}=\sum_{q=1}^{5}\tilde{R}_{i+1/2}^{p,q}\left\{\sum_{s=1}^{5}\tilde{L}_{i+1/2}^{q,s}\left[\begin{array}{l}F_i^{s}\sum_{r=-2}^{3}\left(w_r^{+}+w_r^{-}\right)E_r^{\xi}\left(\frac{\xi_x}{J}\right)_i+G_i^{s}\sum_{r=-2}^{3}\left(w_r^{+}+w_r^{-}\right)E_r^{\xi}\left(\frac{\xi_y}{J}\right)_i \\ +H_i^{s}\sum_{r=-2}^{3}\left(w_r^{+}+w_r^{-}\right)E_r^{\xi}\left(\frac{\xi_z}{J}\right)_i+\alpha U_i^{s}\sum_{r=-2}^{3}\left(w_r^{+}-w_r^{-}\right)E_r^{\xi}\left(\frac{1}{J}\right)_i\end{array}\right]\right\}, \tag{54}
$$

where U^{s}, F^{s}, G^{s} and H^{s} are the $s-th$ component of $\mathbf{U}$, $\mathbf{F}$, $\mathbf{G}$ and $\mathbf{H}$ respectively.
If we define

$$
\begin{aligned}
\tilde{w}_F^{\xi}\left(\phi_i\right)&=\sum_{q=1}^{5}\tilde{R}_{i+1/2}^{p,q}\sum_{s=1}^{5}\tilde{L}_{i+1/2}^{q,s}F_i^{s}\sum_{r=-2}^{3}\left(w_r^{+}+w_r^{-}\right)E_r^{\xi}\left(\phi_i\right) \\
\tilde{w}_G^{\xi}\left(\phi_i\right)&=\sum_{q=1}^{5}\tilde{R}_{i+1/2}^{p,q}\sum_{s=1}^{5}\tilde{L}_{i+1/2}^{q,s}G_i^{s}\sum_{r=-2}^{3}\left(w_r^{+}+w_r^{-}\right)E_r^{\xi}\left(\phi_i\right) \\
\tilde{w}_H^{\xi}\left(\phi_i\right)&=\sum_{q=1}^{5}\tilde{R}_{i+1/2}^{p,q}\sum_{s=1}^{5}\tilde{L}_{i+1/2}^{q,s}H_i^{s}\sum_{r=-2}^{3}\left(w_r^{+}+w_r^{-}\right)E_r^{\xi}\left(\phi_i\right) \\
\tilde{w}_U^{\xi}\left(\phi_i\right)&=\sum_{q=1}^{5}\tilde{R}_{i+1/2}^{p,q}\sum_{s=1}^{5}\tilde{L}_{i+1/2}^{q,s}U_i^{s}\sum_{r=-2}^{3}\left(w_r^{+}-w_r^{-}\right)E_r^{\xi}\left(\phi_i\right)
\end{aligned}, \tag{55}
$$

the numerical flux can be rewritten as

$$
\hat{F}_{i+1/2}^{p}=\tilde{w}_F^{\xi}\left(\frac{\xi_x}{J}\right)_i+\tilde{w}_G^{\xi}\left(\frac{\xi_y}{J}\right)_i+\tilde{w}_G^{\xi}\left(\frac{\xi_z}{J}\right)_i+\tilde{w}_U^{\xi}\left(\frac{1}{J}\right)_i, \tag{56}
$$

In this case, the difference operator δ_1^{ξ} for the $p-th$ component of $\tilde{\mathbf{F}}$ can be written as

$$
\begin{aligned}
\delta_1^{\xi}\tilde{F}^p_{i,j,k} &= \hat{F}^p_{i+1/2,j,k}-\hat{F}^p_{i-1/2,j,k}\\
&= \tilde{w}_F^{\xi}\left(\frac{\xi_x}{J}\right)_{i,j,k}+\tilde{w}_G^{\xi}\left(\frac{\xi_y}{J}\right)_{i,j,k}+\tilde{w}_G^{\xi}\left(\frac{\xi_z}{J}\right)_{i,j,k}+\tilde{w}_U^{\xi}\left(\frac{1}{J}\right)_{i,j,k}\\
&\quad -\tilde{w}_F^{\xi}\left(\frac{\xi_x}{J}\right)_{i-1,j,k}-\tilde{w}_G^{\xi}\left(\frac{\xi_y}{J}\right)_{i-1,j,k}-\tilde{w}_G^{\xi}\left(\frac{\xi_z}{J}\right)_{i-1,j,k}-\tilde{w}_U^{\xi}\left(\frac{1}{J}\right)_{i-1,j,k}
\end{aligned}
\quad , \tag{57}
$$

Thus, $I_x^p\ \left(p=1\sim 5\right)$ can be computed by

$$
\left(I_x^p\right)^N=\frac{1}{F^p}\left\{
\begin{aligned}
&\tilde{w}_F^{\xi}\left(\frac{\xi_x}{J}\right)_{i,j,k}-\tilde{w}_F^{\xi}\left(\frac{\xi_x}{J}\right)_{i-1,j,k}+\tilde{w}_F^{\eta}\left(\frac{\eta_x}{J}\right)_{i,j,k}-\tilde{w}_F^{\eta}\left(\frac{\eta_x}{J}\right)_{i,j-1,k}\\
&+\tilde{w}_F^{\zeta}\left(\frac{\zeta_x}{J}\right)_{i,j,k}-\tilde{w}_F^{\zeta}\left(\frac{\zeta_x}{J}\right)_{i,j,k-1}+\tilde{w}_U^{\xi}\left(\frac{1}{J}\right)_{i,j,k}-\tilde{w}_U^{\xi}\left(\frac{1}{J}\right)_{i-1,j,k}
\end{aligned}
\right\}, \tag{58}
$$

for the characteristic-wise WENO schemes holding freestream. In Eq.(58), $\tilde{w}_F^{\eta}\left(\phi\right)_{i,j,k}$ and $\tilde{w}_F^{\eta}\left(\phi\right)_{i,j-1,k}$ are defined as

$$
\begin{aligned}
\tilde{w}_F^{\eta}\left(\phi_{i,j,k}\right)&=\sum_{q=1}^{5}\tilde{R}^{p,q}_{i,j+1/2,k}\sum_{s=1}^{5}\tilde{L}^{q,s}_{i,j+1/2,k}F^s_{i,j,k}\sum_{r=-2}^{3}\left(w_r^{+}+w_r^{-}\right)E_r^{\eta}\left(\phi_{i,j,k}\right)\\
\tilde{w}_F^{\eta}\left(\phi_{i,j-1,k}\right)&=\sum_{q=1}^{5}\tilde{R}^{p,q}_{i,j-1/2,k}\sum_{s=1}^{5}\tilde{L}^{q,s}_{i,j-1/2,k}F^s_{i,j-1,k}\sum_{r=-2}^{3}\left(w_r^{+}+w_r^{-}\right)E_r^{\eta}\left(\phi_{i,j-1,k}\right)
\end{aligned}
\quad , \tag{59}
$$

where E_r^{η} is the translation operator in $\eta-$direction defined by Eq.(32).

4 Numerical tests

Mesh nonuniformity and nonorthogonality are the major source of geometrically induced errors. Especially in the place where the highly distorted grids or density mutational grids exist, the geometrically induced errors will degrade the fidelity and accuracy of the high order schemes or even cause numerical instabilities. Although we try to generate smooth grids and preserve the computational mesh uniform, grids with distortion and spacing variation are unavoidable in order to fit complex figurations in practical simulations. Therefore, several benchmark test cases which include a uniform flow, an isentropic moving vortex, the double Mach reflection problem and the Rayleigh Taylor instability problem are implemented on various nonuniformity and nonorthogonality grids to assess the freestream preservation properties of the proposed approach. The fifth-order, characteristic-wise WENO scheme with Lax-Friedrichs flux splitting is employed for the space discretization while the third order TVD Runge-Kutta scheme is applied for the time integration. The effectiveness of the strategy is verified by comparing the computational results with those of other schemes. In the following section, the mark “WENO” denotes the standard WENO scheme[4], “WENO-FP” represents the technique proposed by Nonomura et al.[26], “WENO-Like” stands for the WENO schemes with the proposed strategy proposed in the present paper while “Exact” denotes the exact value of the flow fields.

4.1 Uniform flow

A two-dimensional uniform flow is discussed in this subsection. The initialization conditions of the flow are

$$u=U_\infty,\ v=0,\ p=p_\infty$$

with $U_\infty=10$ and $p_\infty=143$.

Firstly, we test the performance of various schemes on two-dimensional distortion-shaped grids as shown in Fig.1. The computational domain is $[-50,50]\times[-50,50]$ and grid number is set to be 100×100. The mesh is bended at $[-40,40]\times[-40,40]$ and it is generated by

$$y_{i,j} = y_{\min} + \Delta y\left[\left(j-1\right) + A\sin\left(n\pi x / L + j\varphi / JL\right)\right], \tag{60}$$

where $y_{i,j}$ is the ordinate value of the point (i,j) and $y_{\min} = -40$ is the initial location of the bended grids. $L = 100$ is the length of the computation domain. JL denotes the mesh number in $\eta-$direction and $\Delta y = L/JL$ represents the grid space before distortion. A, n and φ are the parameters to control the distortion extent and the bending pattern. They are set to be $A = 0.5$, $n = 12$ and $\varphi = 3\pi/2$ respectively in the present test case.

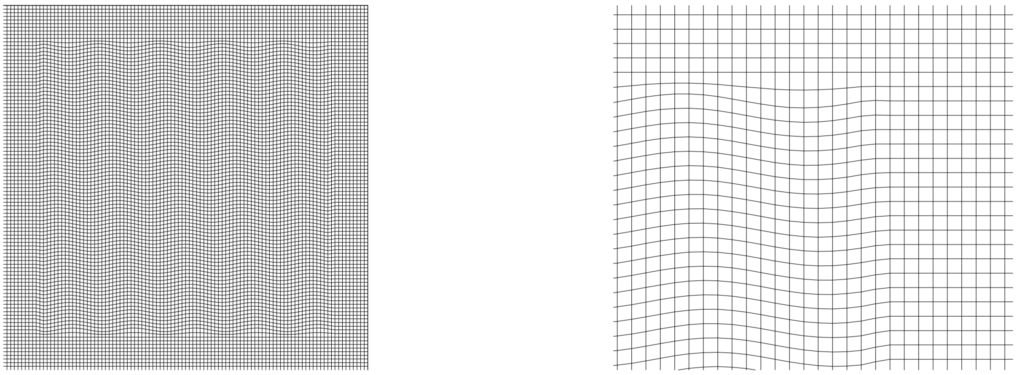

(a) The whole computational domain (b) Enlarged portion of the mesh

Fig. 1 Two-dimensional distortion-shaped grids

Comparisons of the computational results at $t = 0.5$ for various schemes on the two-dimensional distortion-shaped grids are depicted in Fig.2 and Fig.3. Fig.2 shows the pressure contours while Fig.3 presents the distribution of velocities along the central axis and the accumulated L_2 error of the u velocity. It can be clearly noticed that for the traditional WENO scheme, significant errors appear due to the nonuniformity of the mesh and the freestream can not be preserved. The WENO-FP scheme reduces the geometrical induced error at a certain extent while the WENO-Like scheme achieves satisfactory results on this distortion-shaped mesh. Fig 3 denotes that the traditional WENO scheme has large velocities errors in the places with poor quality grids while the WENO-Like scheme has errors less than 10^{-24}, close to machine zero for double-precision computations, which demonstrates that the new strategy can exactly preserve the uniform flow for the distortion-shaped grids.

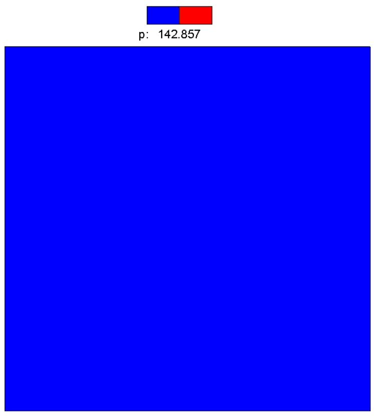

(a) Exact

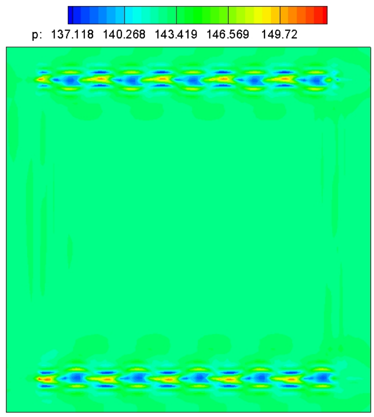

(b) WENO

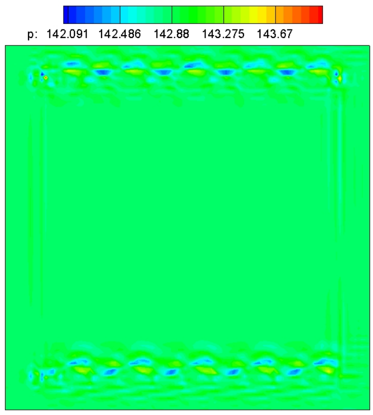

(c) WENO-FP

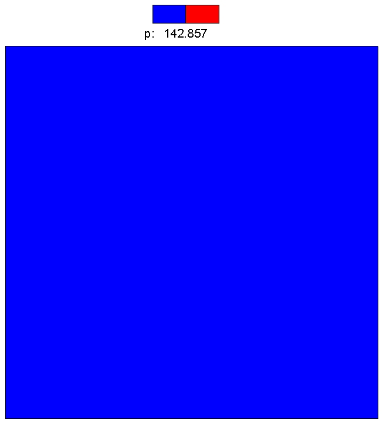

(d) WENO-Like

Fig. 2 Pressure contours of the uniform flow on the two-dimensional distortion-shaped grids

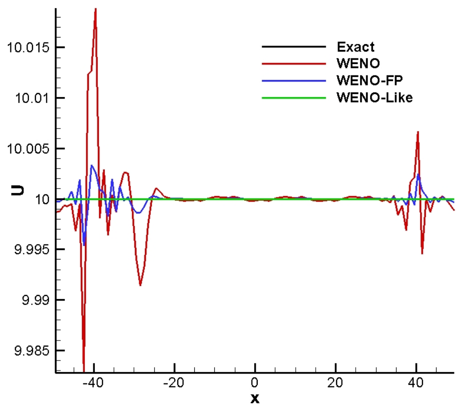

(a) u velocity distributions along the central line of the computational domain

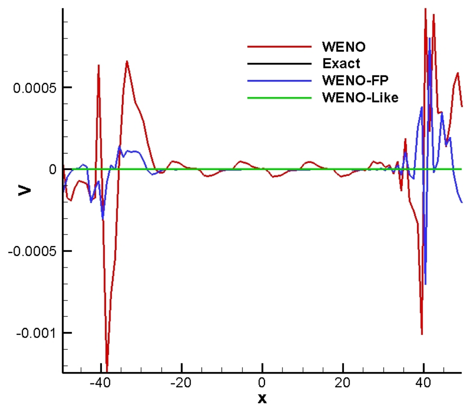

(b) v velocity distributions along the central line of the computational domain

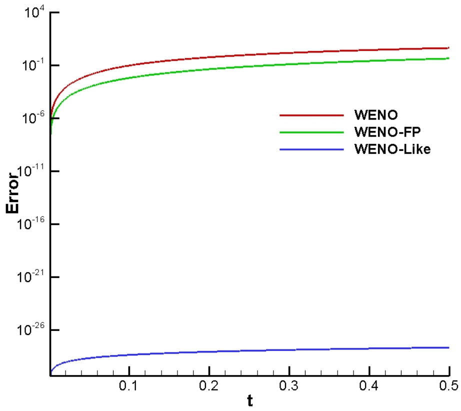

(c) The L_2 error of the u velocity

Fig. 3 Comparisons of the numerical results on the two-dimensional distortion-shaped grids

Next, the freestream preservation properties of the WENO-like scheme are validated on wavy grids as shown in Fig.4 (a). The two-dimensional wavy grids are generated by

$$x_{i,j} = x_{\min} + \Delta x\left[(i-1) + A\cos\left(n\pi\left(y - y_{\min}\right)\right)\right]$$
$$y_{i,j} = y_{\min} + \Delta y\left[(j-1) + A\cos\left(n\pi\left(x - x_{\min}\right)\right)\right],$$

where the parameters are chosen to be $A=3$, n=0.1 . The computational results at $t=0.5$ on 100×100 grid points are shown in Fig.4(b)~ Fig.4(d). For the wavy grids, both the WENO-FP scheme and WENO-like scheme give inspiring results while the numerical errors of WENO scheme are comparably large. When we compare the L_2 errors of the u velocity for the WENO-FP scheme and WENO-like scheme as shown in Fig.4(b), the WENO-Like scheme gives a slightly better results.

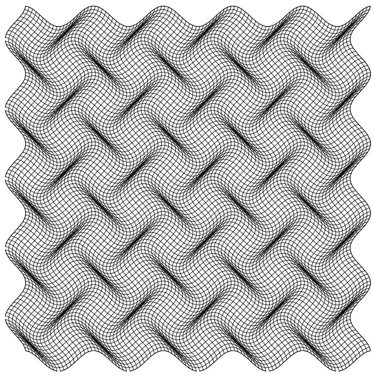

(a) Grids

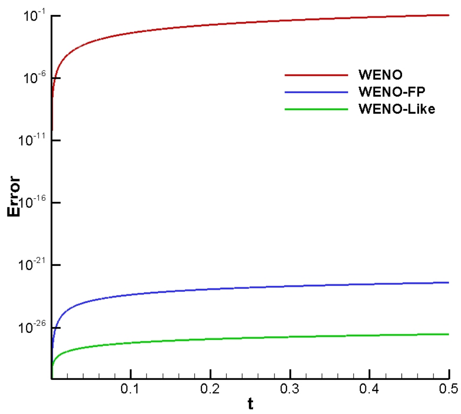

(b) The L_2 error of the u velocity

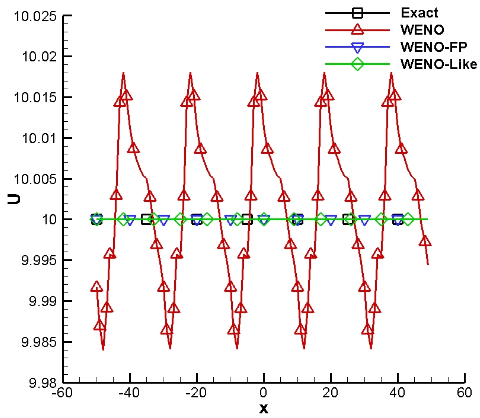

(c) u velocity distributions along the central line of the computational domain

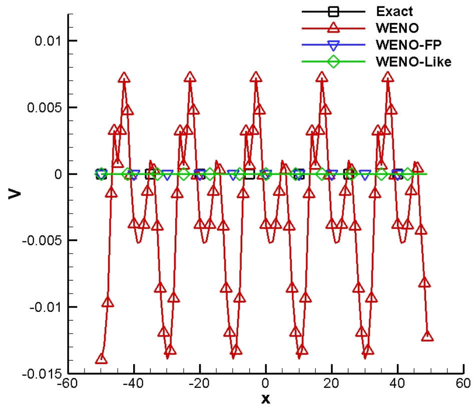

(d) v velocity distributions along the central line of the computational domain

Fig. 3 Comparisons of the numerical results on the two-dimensional wavy grids

Randomly disturbed grids are chosen to further study the properties of the proposed strategy. The distributions of the randomized grids are expressed by

$$x_{i,j} = x_{\min} + \Delta x(i-1) + A\Delta x \operatorname{mod}(i,2) \times random\_number(i)$$
$$y_{i,j} = y_{\min} + \Delta y(i-1) + A\Delta y \operatorname{mod}(j,2) \times random\_number(j),$$

where $random\_number(i)$ and $random\_number(j)$ are random numbers which vary with i and j respectively. $A = 0.9$ is a constant to control the extent of the distortion. The computational domain is chosen to be $[-50,50]\times[-50,50]$ while the random grids are set at the region $[-40,40]\times[-40,40]$ as shown in Fig.5.

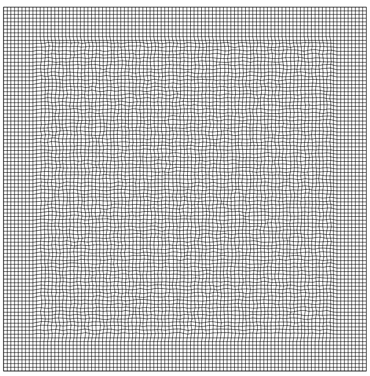

(a) The whole computational domain

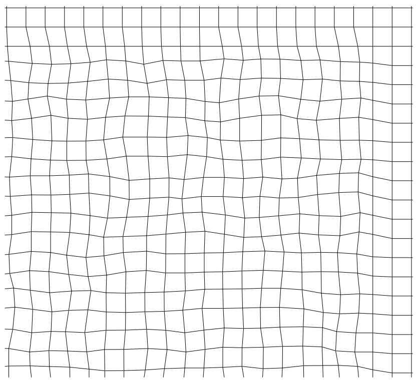

(b) Enlarged portion of the mesh

Fig. 4 Two-dimensional randomized grids

The simulation is implemented on a computational mesh with 100×100 grid points and the results at $t = 0.5$ are shown in Fig.6. These figures demonstrate that results of the WENO scheme have significant errors. Although the results of the WENO-FP scheme are improved compared with that of the WENO scheme, the numerical errors of the velocities are still comparably large. In comparisons, the velocities obtained by WENO-Like scheme are almost the same with the exact ones. These reconfirms that the new strategy can preserve the freestream exactly on various grids, which is consistent with the theoretical analysis in Section 3.

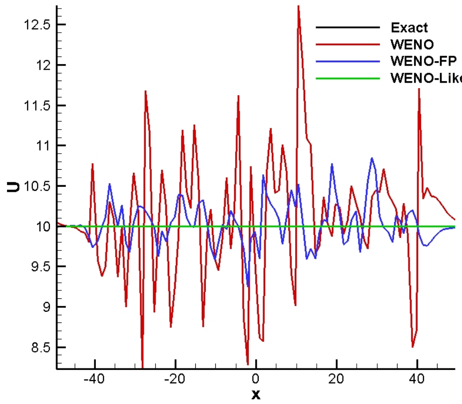

(a) u velocity distributions along the central line of the computational domain

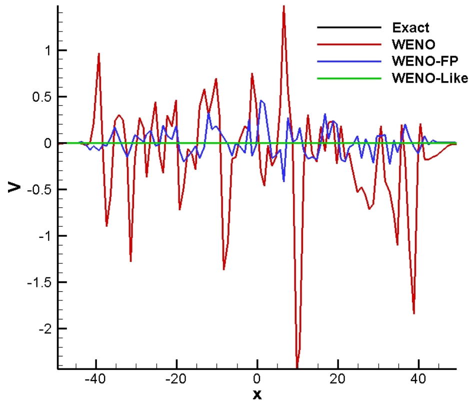

(b) v velocity distributions along the central line of the computational domain

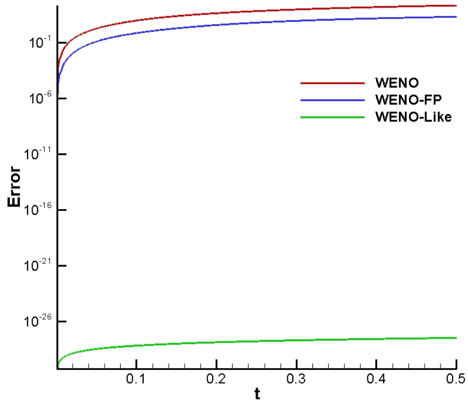

(c) The L_2 error of the u velocity

Fig. 6 Comparisons of the numerical results on the two-dimensional randomized grids

4.2 Moving vortex

In this subsection, the two-dimensional and three-dimensional isentropic moving vortex, which is too weak to bear any relatively large error, are employed to assess the performance of the proposed strategy. An isentropic vortex with freestream Mach number 0.05 located at $(x_c, y_c) = (0,0)$ is chosen as the initial conditions. The velocity and pressure distributions of this vortex are expressed as

$$u = U_\infty - \frac{Cy}{R^2}\exp\left(-r^2/2\right),$$

$$v = \frac{Cx}{R^2}\exp\left(-r^2/2\right),$$

$$p = p_\infty - \frac{\rho C^2}{2R^2}\exp\left(-r^2/2\right),$$

$$r = \sqrt{\frac{x^2+y^2}{R^2}},$$

where $U_\infty = 10$, $C = 2$ and $R = 10$.

This vortex is first computed on the two-dimensional distortion-shaped grids as shown in Fig.1 to assess the vortex preservation properties of various schemes. The simulation is carried up to $t = 0.5$

with 100×100 grid points. Contours of vorticity are shown in Fig.7. The vortices computed by the standard WENO scheme and the WENO-FP scheme are completed covered by the geometrically induced errors, whereas the WENO-Like scheme can preserve the vortex well.

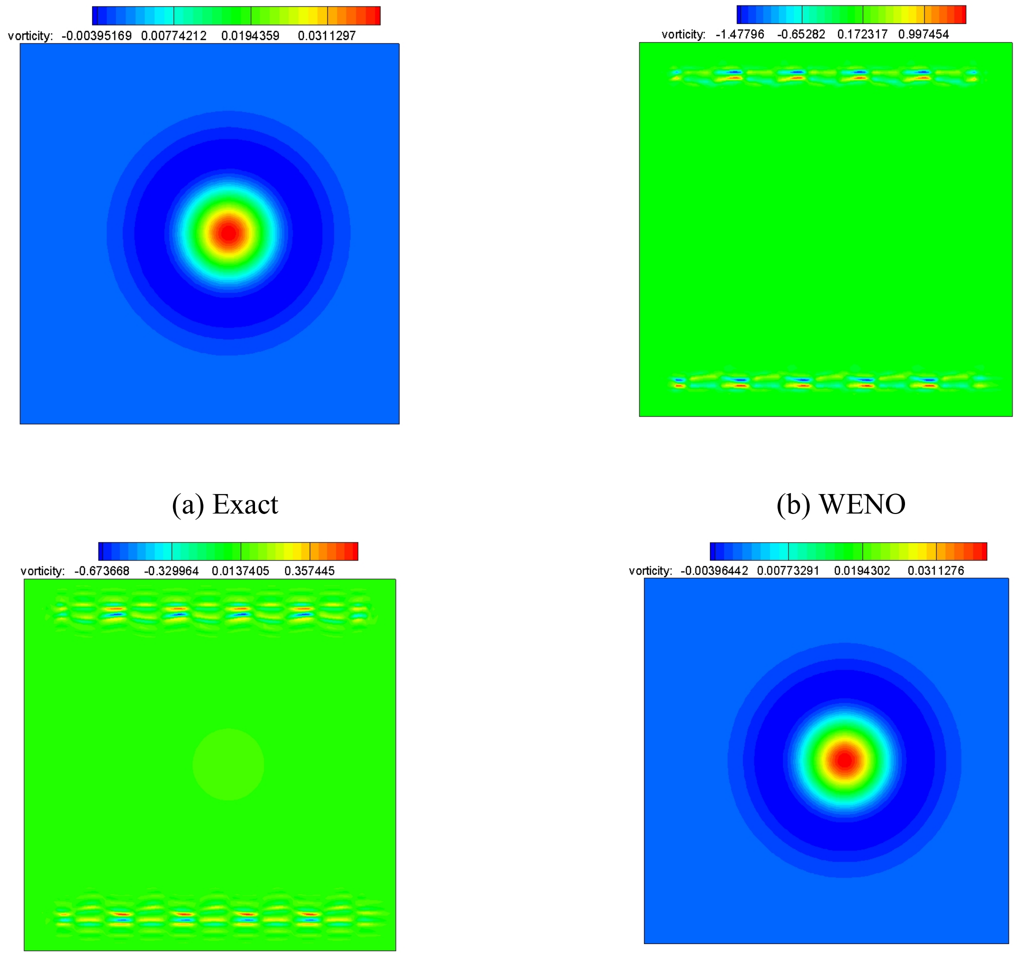

(a) Exact (b) WENO

(c) WENO-FP (d) WENO-Like

Fig. 5 Contours of vorticity for the moving vortex on two-dimensional distortion-shaped grid

Next, the vortex preserving properties of various schemes on the two-dimensional wavy grids are examined. The wavy grids employed for this test case is the same with that for the uniform flow as shown in Fig.4(a). The corresponding results at $t = 0.5$ are depicted in Fig.8. These figures demonstrate that the vortex computed by the standard WENO scheme has comparably large error due to the grid distortion, whereas the vortices computed by WENO-FP scheme and WENO-Like scheme are preserved well compared with the exact solutions.

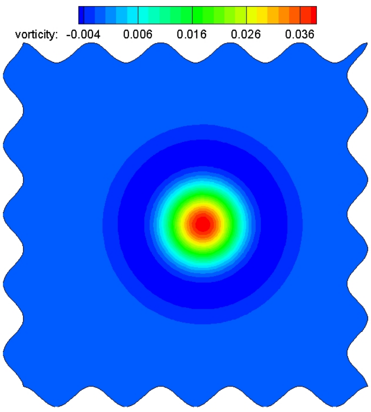

(a) Exact

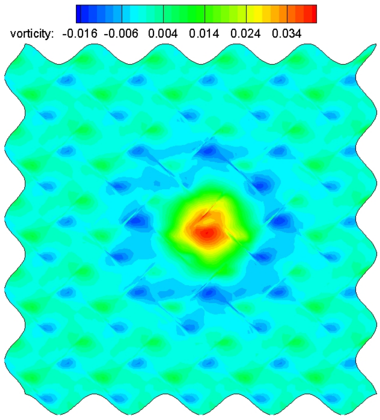

(b) WENO

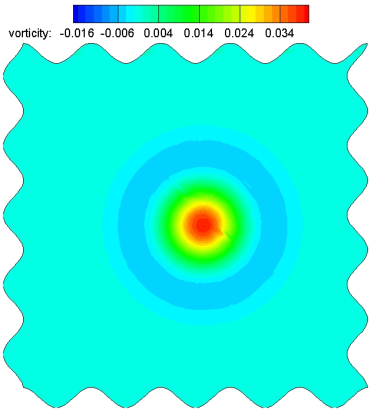

(c) WENO-FP

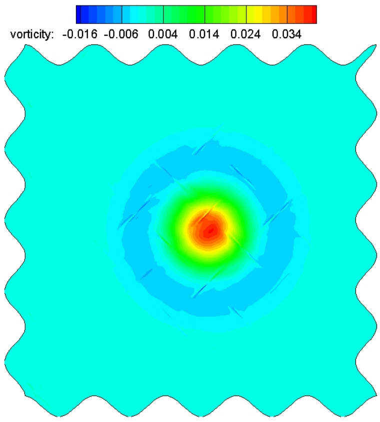

(d) WENO-Like

Fig. 6 Contours of vorticity on the two-dimensional wavy grids

To further study the performance of the WENO-Like scheme on three-dimensional non-uniform grids, the computation of the moving vortex problems is carried out on the three-dimensional space-varying grids as shown in Fig.9. The grids are generated by

$$x_{i,j} = x_{\min} + \Delta x\left(i-1\right) + A\sin\left(n\pi x / L\right)$$
$$y_{i,j} = y_{\min} + \Delta y\left(j-1\right) + A\sin\left(n\pi y / L\right),$$
$$z_{i,j} = z_{\min} + \Delta z\left(k-1\right) + A\sin\left(n\pi z / L\right)$$

where $A = 2,\ n = 2$ and $L = 20$. The computation region is chosen to be $[-40,40]\times[-40,40]\times[-20,20]$ and the simulation is carried out up to $t = 0.3$ with $80\times80\times40$ grid points. Comparisons of the vorticity Contours for the WENO scheme and the WENO-like scheme are shown in Fig.10. It can be clearly observed that the WENO-Like scheme performs well on this three-dimensional space-varying mesh while significant geometrically induced errors cover the real vortex for the standard WENO scheme.

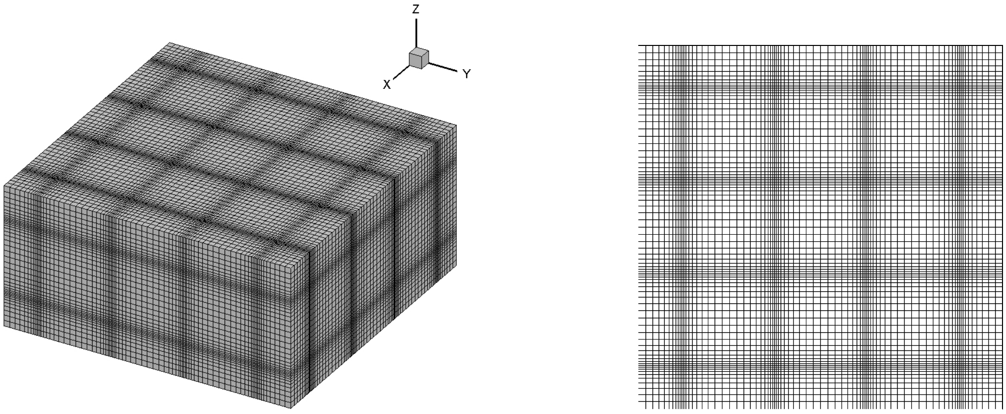

(a) The whole computational domain (b) Local slice of the mesh

Fig. 7 Three-dimensional space-varying grids

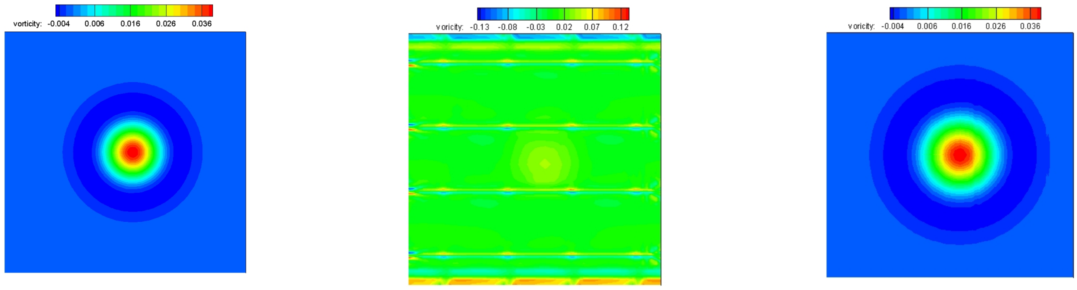

(a) Exact (b) WENO (c) WENO-Like

Fig. 8 Comparisons of vorticity contours on the three-dimensional space-varying grids

4.3 Double Mach reflection problem

Double Mach reflection problem is chosen to examine the performance of the WENO-Like scheme when strong shock waves appear in the flow fields. This problem is solved on a two-dimensional randomized mesh with the computational domain $(x,y)\in[0,4]\times[0,1]$. The initial conditions are given by

$$(\rho,u,v,p)=\begin{cases}1.4,0,0,1.0 & x\geq 1/6+\sqrt{3}/3\,y\\ 8.0,7.1447,-4.125,116.5 & \text{otherwise}\end{cases}.$$

The solution is advanced up to $t=0.2$ with the grid points 400×100. The Courant number is set to be $CFL=0.3$ in the present study. More detailed discussions of this problem can be found, for example, in [27]. The grids are generated by the following equations

$$\begin{aligned}x_{i,j}&=x_{\min}+\Delta x(i-1)+A\Delta x\,\mathrm{mod}(i,2)\bullet random\_number(i)\\ y_{i,j}&=y_{\min}+\Delta y(i-1)+A\Delta y\,\mathrm{mod}(j,2)\bullet random\_number(j)\end{aligned},$$

where A is the coefficient to control the randomness of the grids. Two different random grids with $A=0.1$ and $A=0.5$ is chosen in the present paper. As the parameter A becomes larger, the nonuniformity of the grids becomes more severe. Comparisons of the corresponding density contours for these two grids are shown in Fig.11 and Fig.12 respectively. It can be observed that all the schemes can capture the main features such as the Mach stem and the wall jet. However, it is evident that large non-physical oscillations appear for the standard WENO scheme. Especially for the case $A = 0.5$, the roll up structures of the Kelvin-Helmholtz instability of the slip-line are completely polluted by the non-physical oscillations as shown in Fig.12(b). Both the WENO-FP scheme and the WENO-Like scheme can alleviate these non-physical oscillations. When we compare the results of WENO-Like scheme with those of the WENO-FP scheme, it is obvious the WENO-Like scheme can suppress the oscillations more evidently and thus better results are obtained.

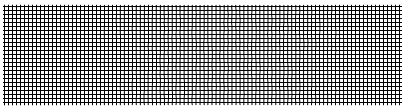

(a) Grids

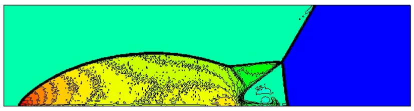

(b) WENO

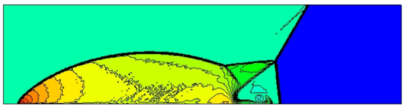

(c) WENO-FP

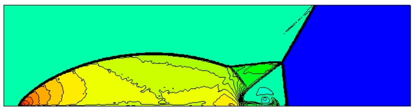

(d) WENO-Like

Fig. 9 Density contours on two-dimensional randomized grids with $A = 0.1$

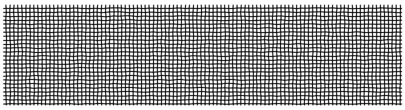

(a) Grids

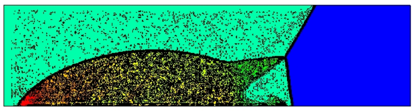

(b) WENO

(c) WENO-FP

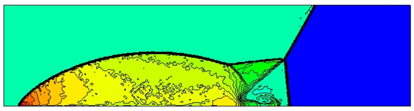

(d) WENO-Like

Fig. 10 Density contours on two-dimensional randomized grid with $A = 0.5$

5 Conclusions

In the present paper, a new numerical strategy for the high order WENO scheme holding freestream on nonuniformity and nonorthogonality grids is proposed. Firstly, we briefly review the coordinate transformation process and the headstream of the geometrical induced errors. Then the flux difference operators of the WENO scheme for the three-dimensional scalar equations are explicitly deduced. Based on the analysis of the WENO operators, we reconfirm the traditional WENO schemes cannot adapt other approaches to satisfy the GCL mainly because the flux discretization operators are nonlinear ones which depend on the difference operators for the metric terms. In order to make the WENO scheme hold freestream, we propose a numerical approach which includes the following steps: (1) The metric invariants in the governing equations are retained and the full forms of the N-S equations on the general curvilinear coordinates are solved; (2) The metric terms are rewritten into the symmetrical conservative form and are discretized by using high order schemes; (3) The evaluation of any outer-level derivatives in geometric invariants is executed by using an upwind-weighted averaging procedure, i.e., the outer-level derivative operators for the metric invariants are kept the same with those for the corresponding inviscid fluxes. This approach is remarked as WENO-Like scheme in the present paper. The fifth-order WENO scheme with Lax-Friedrich flux splitting for the scalar equations is chosen as an example to derive the detailed formulations for the discretization of the metric invariants. Then this approach is extended to solve the Euler and N-S equations by using the component-wise and character-wise WENO schemes. The effectiveness of this approach is validated by implementing several benchmark test cases on various nonuniform grids. Numerical results indicate that when the computational mesh is smooth, both the WENO-FP scheme developed by Nonomera et al. and the proposed WENO-Like scheme can give satisfactory results. However, when the computational mesh is not smooth, i.e., the distortion-shaped grids and the randomized grids appear in the computational domain, the performance of the WENO-Like scheme is much better than that of WENO-FP scheme.

Reference

[1] C. W. Shu. High-order finite difference and finite volume WENO schemes and discontinuous Galerkin methods for CFD. International Journal of Computational Fluid Dynamics, 17(2):107-118, 2003.

[2] S. K. Lele. Compact finite difference schemes with spectral-like resolution. Journal of Computational Physics, 103(1):16-42, 1992.

[3] X. G. Deng, H. X. Zhang. Developing high-order weighted compact nonlinear schemes. Journal of Computational Physics, 165(1):22-44, 2000.

[4] G. S. Jiang, C. W. Shu. Efficient implementation of weighted ENO schemes. Journal of Computational Physics, 126(1):202-228, 1996.

[5] P.D. Thomas, C. K. Lombard. Geometric conservation law and its application to flow computations on moving grids, AIAA Journal, 17 (10): 1030-1037, 1979.

[6] M. Vinokur. An analysis of finite-difference and finite-volume formulations of conservation laws, Journal of Computational Physics, 81: 1-52, 1989.

[7] S. Étienne, A. Garon, D. Pelletier. Perspective on the geometric conservation law and finite element methods for ALE simulations of incompressible flow, Journal of Computational Physics, 228: 2313-2333, 2009.

[8] J.G. Trulio, K.R. Trigger. Numerical solution of the one-dimensional hydrodynamic equations in an arbitrary time-dependent coordinate system, Technical Report UCLR-6522, University of California Lawrence Radiation laboratory, 1961.

[9] H. Zhang, M. Reggio, J.Y. Trépanier, et al. Discrete form of the GCL for moving meshes and its implementation in CFD schemes. Computers & Fluids, 22 (1): 9-23, 1993.

[10] T.H. Pulliam, J.L. Steger. On implicit finite-difference simulations of three-dimensional flow. AIAA Paper 78-10, 1978.

[11] C. Farhat, P. Geuzaine, C. Grandmont. The discrete geometric conservation law and the nonlinear stability of ALE schemes for the solution of flow problems on moving grids. Journal of Computational Physics 174: 669-694, 2001.

[12] D.J. Mavriplis, Z. Yang. Achieving higher-order time accuracy for dynamic unstructured mesh fluid flow simulations: role of the GCL. AIAA Paper, 2005-5114, 2005.

[13] B. Sjögreen, H.C. Yee, M. Vinokur. On high order finite-difference metric discretizations satisfying GCL on moving and deforming grids. Journal of Computational Physics, 265: 211-220, 2014.

[14] R.M. Visbal, D.V. Gaitonde. On the use of higher-order finite-difference schemes on curvilinear and deforming meshes. Journal of Computational Physics, 181: 155-185, 2002.

[15] T. Nonomura, N. Iizuka, K. Fujii. Freestream and vortex preservation properties of high-order WENO and WCNS on curvilinear grids. Computers & Fluids, 39: 197-214, 2010.

[16] X.G. Deng, M.L. Mao, G.H. Tu, et al. Geometric conservation law and applications to high-order finite difference schemes with stationary grids. Journal of Computational Physics, 230: 1100-1115, 2011.

[17] X.G. Deng, Y.B. Min, M.L. Mao, et al. Further studies on geometric conservation law and applications to high-order finite difference schemes with stationary grids. Journal of Computational Physics, 239: 90-111, 2013.

[18] Y. Abe, N. Iizuka, T. Nonomura, et al. Conservative metric evaluation for high-order finite

difference schemes with the GCL identities on moving and deforming grids. Journal of Computational Physics, 232: 14-21, 2013.
[19] Y. Abe, T. Nonomura, N. Iizuka, et al. Geometric interpretations and spatial symmetry property of metrics in the conservative form for high-order finite difference schemes on moving and deforming grids. Journal of Computational Physics, 260: 163-203, 2014.
[20] F Liao, Z.Y. Zhang, L.X. Zhang. Extending geometric conservation law to cell-centered finite difference methods on stationary grids. Journal of Computational Physics, 284: 419-433, 2014.
[21] X.D. Deng, Y. Jiang, M.L. Mao, et al. A family of hybrid cell-edge and cell-node dissipative compact schemes satisfying geometric conservation law. Computers & Fluids, 116: 29-45, 2015.
[22] X. Cai, F. Ladeinde. Performance of WENO scheme in generalized curvilinear coordinate systems. AIAA Paper 2008-36, 2008.
[23] Y. Jiang, C.W. Shu, M. Zhang. An alternative formulation of finite difference weighted ENO schemes with Lax-Wendroff time discretization for conservation laws. SIAM Journal of Scientific Computing, 35(2):1137-60, 2013.
[24] Y. Jiang, C.W. Shu, M. Zhang. Free-stream preserving finite difference schemes on curvilinear meshes. Brown University, Scientific Computing Group Report 2013-10. Brown University; 2013.
[25] M. Asahara, T. Nonomura, K. Fujii, et al. Comparison of resolution and robustness with TSFDWENO schemes. Proceedings of (Japanese) 27th computational fluid dynamics symposium, C03-4, 2013. [in Japanese].
[26] T. Nonomura, D. Terakado, Y. Abe, et al. A new technique for freestream preservation of finite-difference WENO on curvilinear grid, Computers & Fluids, 107: 242-255, 2015.
[27] P.Woodward, P. Colella. The numerical simulation of two-dimensional fluid flow with strong shocks. Journal of Computational Physics, 54: 115-173, 1984.